astro-ph/0301505
UMN–TH–2127/03
TPI–MINN–03/02
January 2003

TASI LECTURES ON DARK MATTER*

KEITH A. OLIVE†
William I. Fine Theoretical Physics Institute, School of Physics and Astronomy, University of Minnesota, Minneapolis, MN 55455 USA
E-mail: olive@umn.edu

Observational evidence and theoretical motivation for dark matter are presented and connections to the CMB and BBN are made. Problems for baryonic and neutrino dark matter are summarized. Emphasis is placed on the prospects for supersymmetric dark matter.

1. Lecture 1

The nature and identity of the dark matter of the Universe is one of the most challenging problems facing modern cosmology. The problem is a long-standing one, going back to early observations of mass-to-light ratios by Zwicky[1]. Given the distribution (by number) of galaxies with total luminosity L, $\phi(L)$, one can compute the mean luminosity density of galaxies

$$\mathcal{L} = \int L\phi(L)dL \tag{1}$$

which is determined to be[2]

$$\mathcal{L} \simeq 2 \pm 0.2 \times 10^8 h_o L_\odot Mpc^{-3} \tag{2}$$

where $L_\odot = 3.8 \times 10^{33}$ erg s^{-1} is the solar luminosity. In the absence of a cosmological constant, one can define a critical energy density, $\rho_c = 3H^2/8\pi G_N = 1.88 \times 10^{-29} {h_o}^2$ g cm^{-3}, such that $\rho = \rho_c$ for three-space curvature $k = 0$, where the present value of the Hubble parameter has been defined by $H_o = 100 h_o$ km Mpc^{-1} s^{-1}. We can now define a critical mass-to-light ratio is given by

$$(M/L)_c = \rho_c/\mathcal{L} \simeq 1390 h_o (M_\odot/L_\odot) \tag{3}$$

*Summary of lectures given at the Theoretical Advanced Study Institute in Elementary Particle Physics at the University of Colorado at Boulder - June 2-28, 2002.

†This work was supported in part by DOE grant DE-FG02-94ER40823 at Minnesota.

which can be used to determine the cosmological density parameter

$$\Omega_m = \frac{\rho}{\rho_c} = (M/L)/(M/L)_c \tag{4}$$

Mass-to-light ratios are, however, strongly dependent on the distance scale on which they are determined[3]. In the solar neighborhood $M/L \simeq 2 \pm 1$ (in solar units), yielding values of Ω_m of only $\sim .001$. In the bright central parts of galaxies, $M/L \simeq (10-20)h_o$ so that $\Omega_m \sim 0.01$. On larger scales, that of binaries and small groups of galaxies, $M/L \sim (60-180)h_o$ and $\Omega_m \simeq 0.1$. On even larger scales, that of clusters, M/L may be as large as $(200-500)h_o$ giving $\Omega_m \simeq 0.3$. This progression in M/L seems to have halted, as even on the largest scales observed today, mass-to-light ratios imply values of $\Omega_m \lesssim 0.3-0.4$. Thus when one considers the scale of galaxies (and their halos) and larger, the presence of dark matter (and as we shall see, non-baryonic dark matter) is required.

Direct observational evidence for dark matter is found from a variety of sources. On the scale of galactic halos, the observed flatness of the rotation curves of spiral galaxies is a clear indicator for dark matter. There is also evidence for dark matter in elliptical galaxies, as well as clusters of galaxies coming from the X-ray observations of these objects. Also, direct evidence has been obtained through the study of gravitational lenses. On the theoretical side, we predict the presence of dark matter (or dark energy) because 1) it is a strong prediction of most inflation models (and there is at present no good alternative to inflation) and 2) our current understanding of galaxy formation requires substantial amounts of dark matter to account for the growth of density fluctuations. One can also make a strong case for the existence of non-baryonic dark matter in particular. The recurrent problem with baryonic dark matter is that not only is it very difficult to hide baryons, but given the amount of dark matter required on large scales, there is a direct conflict with primordial nucleosynthesis if all of the dark matter is baryonic. In this first lecture, I will review the observational and theoretical evidence supporting the existence of dark matter.

1.1. *Observational Evidence*

Assuming that galaxies are in virial equilibrium, one expects that one can relate the mass at a given distance r, from the center of a galaxy to its rotational velocity by

$$M(r) \propto v^2 r/G_N \tag{5}$$

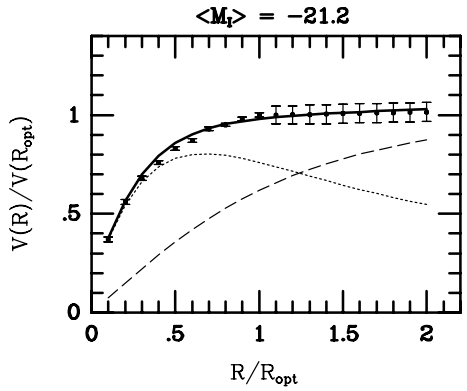

Figure 1. Synthetic rotation curve[5] for galaxies with $\langle M \rangle = -21.2$. The dotted curve shows the disk contribution, whereas the dashed curve shows the halo contribution.

The rotational velocity, v, is measured[3,4] by observing 21 cm emission lines in HI regions (neutral hydrogen) beyond the point where most of the light in the galaxy ceases. A subset of a compilation[5] of nearly 1000 rotation curves of spiral galaxies is shown in Fig. 1. The subset shown is restricted to a narrow range in brightness, but is characteristic for a wide range of spiral galaxies. Shown is the rotational velocity as a function of r in units of the optical radius. If the bulk of the mass is associated with light, then beyond the point where most of the light stops, M would be constant and $v^2 \propto 1/r$. This is not the case, as the rotation curves appear to be flat, i.e., $v \sim$ constant outside the core of the galaxy. This implies that $M \propto r$ beyond the point where the light stops. This is one of the strongest pieces of evidence for the existence of dark matter. Velocity measurements indicate dark matter in elliptical galaxies as well[6].

Galactic rotation curves are not the only observational indication for the existence of dark matter. X-ray emitting hot gas in elliptical galaxies also provides an important piece of evidence for dark matter. A particularly striking example is that of the large elliptical M87. Detailed profiles of the temperature and density of the hot X-ray emitting gas have been mapped out[7]. Assuming hydrostatic equilibrium, these measurements allow one to determine the overall mass distribution in the galaxy necessary to bind the hot gas. Based on an isothermal model with temperature $kT = 3$keV (which leads to a conservative estimate of the total mass), Fabricant and Gorenstein[7] predicted that the total mass out to a radial distance of 392 kpc is $5.7 \times 10^{13} M_\odot$, whereas the mass in the hot gas is only $2.8 \times 10^{12} M_\odot$

or only 5% of the total. The visible mass is expected to contribute only 1% of the total.

M87 is not the only example of an elliptical galaxy in which X-ray emitting hot gas is observed to indicate the presence of dark matter. X-ray observations have shown that the total mass associated with elliptical galaxies is considerably larger than the luminous component in many examples of varying morphological types[8]. Mass-to-light ratios for these systems vary, with most being larger than $30h_0$ and some ranging as high as $\sim 200h_0$.

In addition, similar inferences pertaining to the existence of dark matter can be made from the X-ray emission from small groups of galaxies[9]. On these scales, mass-to-light ratios are typically $\gtrsim 100h_0$ and detailed studies have shown that the baryon faction in these systems is rather small. Furthermore, it was argued[10] that cluster baryon fractions should not differ from the Universal value given by Ω_B/Ω_m. Using an estimate of $\Omega_B = 0.04$ from big bang nucleosynthesis (BBN, see below), and baryon fractions ranging from 0.1 to 0.3, one would obtain an estimate for the total matter density of 0.13 – 0.4.

Another piece of evidence on large scales is available from gravitational lensing[11]. The systematic lensing of the roughly 150,000 galaxies per deg^2 at redshifts between $z = 1 - 3$ into arcs and arclets allow one to trace the matter distribution in a foreground cluster. Lensing observations can be categorized as either strong (multiple images) or weak (single images). Both require the presence of a dominant dark matter component.

Strong lensing is particularly adept in testing the overall geometry of the Universe[12,13]. While a cluster which provides multiple lenses of a single background galaxy (at known redshift) is useful for determining the total cluster mass, when several background galaxies are lensed, it is possible to constrain the values of Ω_m and Ω_Λ [14]. The recent results of [13] show a degeneracy in the Ω_m – Ω_Λ plane. Nevertheless, the allowed region is offset from similar types of degeneracies found in supernovae searches and the CMB (see below). Indeed, these lensing results are much more constraining in Ω_m than the other techniques, though a residual uncertainty of about 30 % persists. While in principle, these results find that any value (from 0 to 1) is possible for Ω_Λ, $\Omega_m < 0.5$ for low values of Ω_Λ and $\Omega_m < 0.4$ for higher values of Ω_Λ ($\gtrsim 0.6$).

Weak lensing of galaxies by galaxies can (on a statistical basis) also probe the nature of galactic halos. Recent studies based on weak lensing data indicate that galactic halos may be far more extended than previously thought[15] (radii larger than 200 h_0^{-1} kpc). These results also imply a sub-

stantial contribution to Ω_m (of order 0.1-0.2) on this scale. On larger scales, using many cluster lenses enables one to estimate $\Omega \simeq 0.3$ [16]. Another use of weak lensing statistics is to determine the evolution of cosmic shear and hence an estimate of Ω_m [17]. Finally, there exist a number of examples of dark clusters, ie., lenses with no observable counterpart[18]. The contribution of these objects (if they are robust) to Ω_m is not clear. For a recent review of weak lensing see [19].

Finally, on very large scales, it is possible to get an estimate of Ω_m from the distribution of peculiar velocities of galaxies and clusters. On scales, λ, where perturbations, δ, are still small, peculiar velocities can be expressed[20] as $v \sim H\lambda\delta\Omega_m^{0.6}$. On these scales, older measurements of the peculiar velocity field from the IRAS galaxy catalogue indicate that indeed Ω is close to unity[21]. Some of the new data indicates a lower value in the range[22] 0.2 – 0.5, but does not conclusively exclude $\Omega_m = 1$ [23].

The above discussion of observational evidence for dark matter pertains largely to the overall matter density of the Universe Ω_m. (For a comprehensive review of determinations of the matter density, see ref. [24].) However, the matter density and the overall *curvature* are not related one-to-one. The expansion rate of the Universe in the standard FRW model is expressed by the Friedmann equation

$$H^2 = \frac{\dot{R}^2}{R^2} = \frac{8\pi G_N \rho}{3} - \frac{k}{R^2} + \frac{\Lambda}{3} \tag{6}$$

where $R(t)$ is the cosmological scale factor, k is the three-space curvature constant ($k = 0, +1, -1$ for a spatially flat, closed or open Universe), and Λ is the cosmological constant. The Friedmann equation can be rewritten as

$$(\Omega - 1)H^2 = \frac{k}{R^2} \tag{7}$$

so that $k = 0, +1, -1$ corresponds to $\Omega = 1, \Omega > 1$ and $\Omega < 1$. However, the value of Ω appearing in Eq. (7) represents the sum $\Omega = \Omega_m + \Omega_\Lambda$ of contributions from the matter density (Ω_m) and the cosmological constant ($\Omega_\Lambda = \Lambda/3H^2$).

There has been a great deal of progress in the last several years concerning the determination of both Ω_m and Ω_Λ. Cosmic Microwave Background (CMB) anisotropy experiments have been able to determine the curvature (i.e. the sum of Ω_m and Ω_Λ) to with in about 10%, while observations of type Ia supernovae at high redshift provide information on a (nearly) orthogonal combination of the two density parameters.

The CMB is of course deeply rooted in the development and verification of the big bang model[25]. Indeed, it was the formulation of BBN that led to the prediction of the microwave background. The argument is rather simple. BBN requires temperatures greater than 100 keV, which according to the standard model time-temperature relation, $t_s T_{\rm MeV}^2 = 2.4/\sqrt{N}$, where N is the number of relativistic degrees of freedom at temperature T, and corresponds to timescales less than about 200 s. The typical cross section for the first link in the nucleosynthetic chain is

$$\sigma v(p + n \rightarrow D + \gamma) \simeq 5 \times 10^{-20} {\rm cm}^3/{\rm s} \tag{8}$$

This implies that it was necessary to achieve a density

$$n \sim \frac{1}{\sigma v t} \sim 10^{17} {\rm cm}^{-3} \tag{9}$$

for nucleosynthesis to begin. The density in baryons today is known approximately from the density of visible matter to be $n_{Bo} \sim 10^{-7}$ cm^{-3} and since we know that that the density n scales as $R^{-3} \sim T^3$, the temperature today must be

$$T_o = (n_{Bo}/n)^{1/3} T_{\rm BBN} \sim 10{\rm K} \tag{10}$$

thus linking two of the most important tests of the Big Bang theory.

Microwave background anisotropy measurements have made tremendous advances in the last few years. The power spectrum[26,27,28] has been measured relatively accurately out to multipole moments corresponding to $\ell \sim 1000$. The details of this spectrum enable one to make accurate predictions of a large number of fundamental cosmological parameters[27,29,30,31,32,33]. An example of these results as found by a recent frequentist analysis[34] is shown in Fig. 2.

Of particular interest to us here is the CMB determination of the total density, $\Omega_{\rm tot}$, as well as the matter density Ω_m. The results of recent CMB anisotropy measurements are summarized in Table 1. As one can see, there is strong evidence that the Universe is flat or very close to it. Furthermore, the matter density is very consistent with the observational determinations discussed above and the baryon density, as we will see below, is consistent with the BBN production of D/H and its abundance in quasar absorption systems.

The discrepancy between the CMB value of Ω_m and Ω_B is sign that non-baryonic matter (dark matter) is required. Furthermore, the apparent discrepancy between the CMB value of $\Omega_{\rm tot}$ and Ω_m, though not conclusive on its own, is a sign that a contribution from the vacuum energy density or

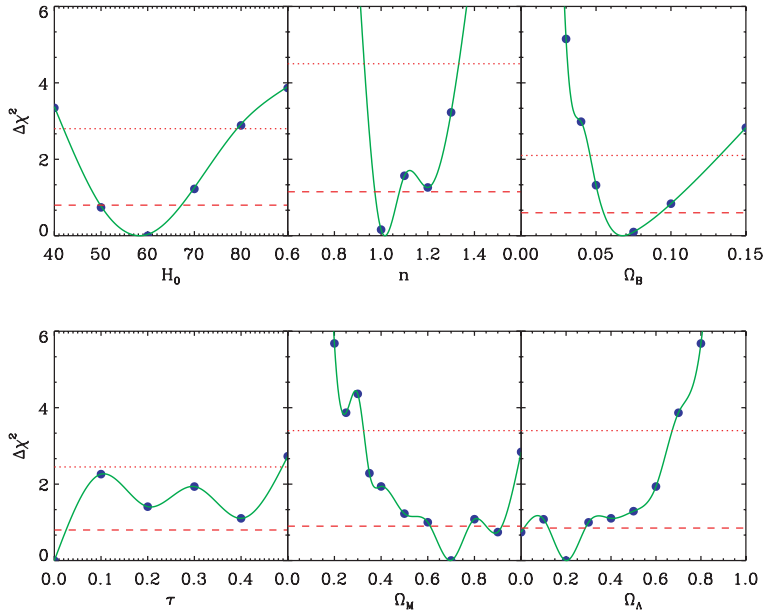

Figure 2. $\Delta\chi^2$ calculated with the MAXIMA-1 and COBE data as a function of parameter value. Solid blue circles show grid points in parameter space, and the green lines were obtained by interpolating between grid points. The parameter values where the green line intercepts the red dashed (dotted) line corresponds to the 68% (95%) frequentist confidence region[34].

Table 1. Results from recent CMB anisotropy measurements.

	$\Omega_{\rm tot}$	$\Omega_m h^2$	$\Omega_B h^2$
BOOMERanG[27]	1.03 ± 0.06	0.12 ± 0.05	$0.021^{+0.004}_{-0.003}$
MAXIMA[29]	$0.9^{+0.09}_{-0.08}$	$0.17^{+0.08}_{-0.04}$	0.0325 ± 0.0125
MAXIMA (freq.)[34]	$0.89^{+0.13}_{-0.10}$	$0.25^{+0.07}_{-0.09}$	$0.026^{+0.010}_{-0.006}$
DASI[30]	1.04 ± 0.06	0.14 ± 0.04	$0.022^{+0.004}_{-0.003}$
CBI[31]	0.99 ± 0.12	$0.17^{+0.08}_{-0.06}$	$0.022^{+0.015}_{-0.009}$
VSA[32]	1.03 ± 0.012	$0.13^{+0.08}_{-0.05}$	0.029 ± 0.009
Archeops[33]	$1.16^{+0.24}_{-0.20}$	–	$0.019^{+0.006}_{-0.007}$

cosmological constant, is also required. The preferred region in the $\Omega_m - \Omega_\Lambda$ plane as determined by a frequentist analysis of MAXIMA data is shown in Fig. 3.

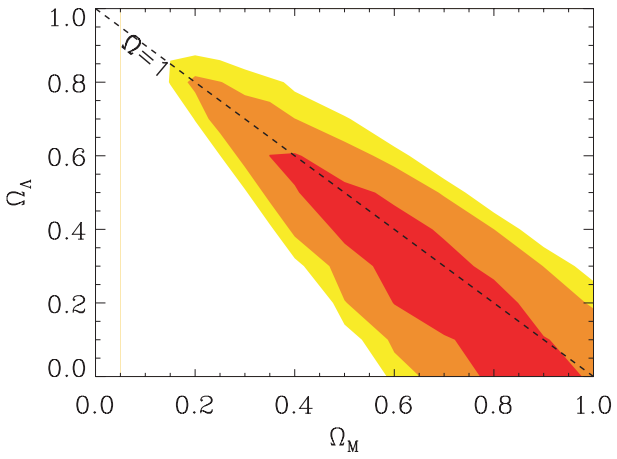

Figure 3. Two-dimensional frequentist confidence regions in the $(\Omega_{\rm M}, \Omega_\Lambda)$ plane. The red, orange and yellow regions correspond to the 68%, 95%, and 99% confidence regions respectively. The dashed black line corresponds to a flat universe, $\Omega = \Omega_m + \Omega_\Lambda = 1$.

The presence or absence of a cosmological constant is a long standing problem in cosmology. To theorists, it is particularly offensive due to the necessary smallness of the constant. We know that the cosmological term is at most a factor of a few times larger than the current mass density. Thus from Eq. (6), we see that the dimensionless combination, $G_N\Lambda \lesssim 10^{-121}$. Nevertheless, even a small non-zero value for Λ could greatly affect the future history of the Universe: allowing open Universes to recollapse (if $\Lambda < 0$), or closed Universes to expand forever (if $\Lambda > 0$ and sufficiently large).

Another exciting development has been the use of type Ia supernovae, which now allow measurement of relative distances with 5% precision. In combination with Cepheid data from the HST key project on the distance scale, SNe results are the dominant contributor to the best modern value for H_0: $72\,{\rm km\,s^{-1}Mpc^{-1}} \pm 10\%$ [35]. Better still, the analysis of high-z SNe has allowed the first meaningful test of cosmological geometry to be carried out, as shown in Fig. 4.

These results can be contrasted with those from the CMB anisotropy measurements as in Fig. 5. We are led to a seemingly conclusive picture. The Universe is nearly flat with $\Omega_{\rm tot} \simeq 1$. However the density in matter makes up only 20-50% of this total, with the remainder in a cosmological constant or some other form of dark energy.

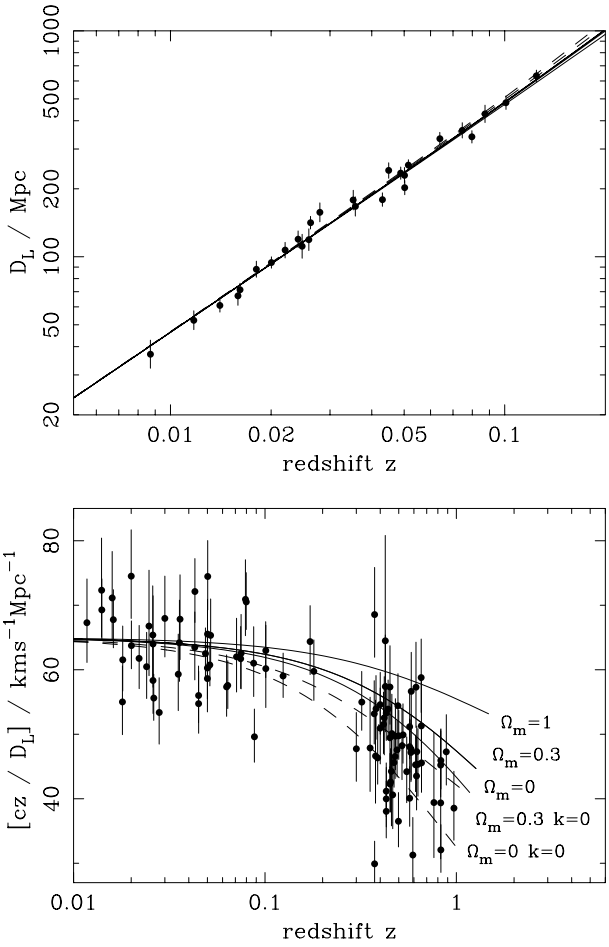

Figure 4. The type Ia supernova Hubble diagram[36] taken from [37]. The first panel shows that, for $z \ll 1$, the large-scale Hubble flow is indeed linear and uniform; the second panel shows an expanded scale, with the linear trend divided out, and with the redshift range extended to show how the Hubble law becomes nonlinear. Comparison with the prediction of Friedmann-Lemaître models appears to favor a vacuum-dominated universe.

1.2. *Theory*

Theoretically, there is no lack of support for the dark matter hypothesis. The standard big bang model including inflation almost requires $\Omega_{\rm tot} = 1$ [38]. This can be seen from the following simple solution to the curvature problem. The simple and unfortunate fact that at present we do not even

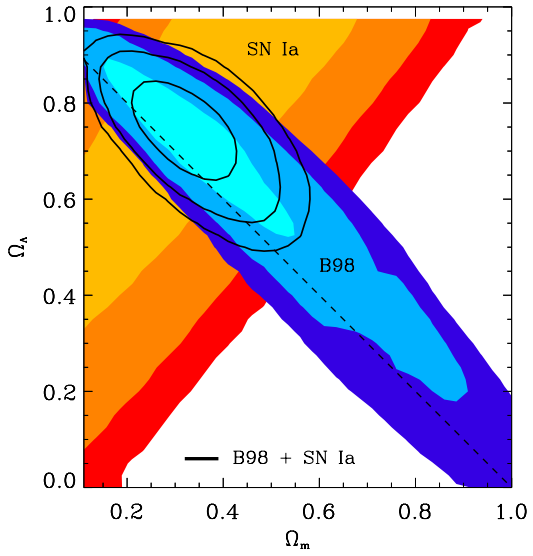

Figure 5. Likelihood-based confidence contours[27] over the plane Ω_Λ (i.e. Ω_v assuming $w = -1$ vs Ω_m. The SNe Ia results very nearly constrain $\Omega_v - \Omega_m$, whereas the results of CMB anisotropies (from the Boomerang 98 data) favor a flat model with $\Omega_v + \Omega_m \simeq 1$. The intersection of these constraints is the most direct (but far from the only) piece of evidence favoring a flat model with $\Omega_m \simeq 0.3$.

know whether Ω is larger or smaller than one, indicates that we do not know the sign of the curvature term further implying that it is subdominant in Eq. (6)

$$\frac{k}{R^2} < \frac{8\pi G}{3}\rho \tag{11}$$

In an adiabatically expanding Universe, $R \sim T^{-1}$ where T is the temperature of the thermal photon background. Therefore the quantity

$$\hat{k} = \frac{k}{R^2T^2} < \frac{8\pi G}{3T_o^2} < 2 \times 10^{-58} \tag{12}$$

is dimensionless and constant in the standard model. This is known as the curvature problem and can be resolved by a period of inflation. Before inflation, let us write $R = R_i$, $T = T_i$ and $R \sim T^{-1}$. During inflation, $R \sim T^{-1} \sim e^{Ht}$, where H is constant. After inflation, $R = R_f \gg R_i$ but $T = T_f = T_R \lesssim T_i$ where T_R is the temperature to which the Universe reheats. Thus $R \not\sim T$ and $\hat{k} \to 0$ is not constant. But from Eqs. (7) and

(12) if $\hat{k} \to 0$ then $\Omega \to 1$, and since typical inflationary models contain much more expansion than is necessary, Ω becomes exponentially close to one.

The inflationary prediction of $\Omega = 1$ is remarkably consistent with the CMB measurements discussed above. Furthermore, we know two things: Dark matter exists, since we don't see $\Omega = 1$ in luminous objects, and most (about 90%) of the dark matter is not baryonic. The latter conclusion is a result of our forthcoming discussion on BBN which constrains the baryon-to-photon ratio and hence Ω_B. Thus $1 - \Omega_B$ is not only dark but also non-baryonic. Furthermore, the matter density is surely composed of several contributions: $\Omega_m = \Omega_B + \Omega_\nu + \Omega_\chi$ where the latter represents the dark matter contribution.

Another important piece of theoretical evidence for dark matter comes from the simple fact that we are living in a galaxy. The type of perturbations produced by inflation[39] are, in most models, adiabatic perturbations ($\delta\rho/\rho \propto \delta T/T$), and I will restrict my attention to these. Indeed, the perturbations produced by inflation also have the very nearly scale-free spectrum described by Harrison and Zeldovich[40]. When produced, scale-free perturbations fall off as $\frac{\delta\rho}{\rho} \propto l^{-2}$ (increase as the square of the wave number). At early times $\delta\rho/\rho$ grows as t until the time when the horizon scale (which is proportional to the age of the Universe) is comparable to l. At later times, the growth halts (the mass contained within the volume l^3 has become smaller than the Jean's mass) and $\frac{\delta\rho}{\rho} = \delta$ (roughly) independent of the scale l. When the Universe becomes matter dominated, the Jean's mass drops dramatically and growth continues as $\frac{\delta\rho}{\rho} \propto R \sim 1/T$.

The transition to matter dominance is determined by setting the energy densities in radiation (photons and any massless neutrinos) equal to the energy density in matter (baryons and any dark matter). For three massless neutrinos and baryons (no dark matter), matter dominance begins at

$$T_m = 0.22 m_B \eta \tag{13}$$

and for $\eta < 7 \times 10^{-10}$, this corresponds to $T_m < 0.14$ eV.

Because we are considering adiabatic perturbations, there will be anisotropies produced in the microwave background radiation on the order of $\delta T/T \sim \delta$. The value of δ, the amplitude of the density fluctuations at horizon crossing, has been determined by COBE[41], $\delta = (5.7 \pm 0.4) \times 10^{-6}$. Without the existence of dark matter, $\delta\rho/\rho$ in baryons could then achieve a maximum value of only $\delta\rho/\rho \sim A_\lambda \delta (T_m/T_o) \lesssim 2 \times 10^{-3} A_\lambda$, where $T_o = 2.35 \times 10^{-4}$ eV is the present temperature of the microwave back-

ground and $A_\lambda \sim 1-10$ is a scale dependent growth factor. The overall growth in $\delta\rho/\rho$ is too small to argue that growth has entered a nonlinear regime needed to explain the large value (10^5) of $\delta\rho/\rho$ in galaxies.

Dark matter easily remedies this dilemma in the following way. The transition to matter dominance is determined by setting equal to each other the energy densities in radiation (photons and any massless neutrinos) and matter (baryons and any dark matter). While if we suppose that there exists dark matter with an abundance $Y_\chi = n_\chi/n_\gamma$ (the ratio of the number density of χ's to photons) then

$$T_m = 0.22 m_\chi Y_\chi \tag{14}$$

Since we can write $m_\chi Y_\chi/\mathrm{GeV} = \Omega_\chi h^2/(4\times 10^7)$, we have $T_m/T_o = 2.4\times 10^4 \Omega_\chi h^2$ which is to be compared with 600 in the case of baryons alone. The baryons, although still bound to the radiation until decoupling, now see deep potential wells formed by the dark matter perturbations to fall into and are no longer required to grow at the rate $\delta\rho/\rho \propto R$.

With regard to dark matter and galaxy formation, all forms of dark matter are not equal. They can be distinguished by their relative temperature at T_m [42]. Particles which are still largely relativistic at T_m (like neutrinos or other particles with $m_\chi < 100$ eV) have the property[43] that (due to free streaming) they erase perturbations out to very large scales given by the Jean's mass

$$M_J = 3\times 10^{18}\frac{M_\odot}{{m_\chi}^2(eV)} \tag{15}$$

Thus, very large scale structures form first and galaxies are expected to fragment out later. Particles with this property are termed hot dark matter particles. Cold particles ($m_\chi > 1$ MeV) have the opposite behavior. Small scale structure forms first aggregating to form larger structures later. It is now well known that pure HDM cosmologies can not reproduce the observed large scale structure of the Universe. In contrast, CDM does much better. Current attention is focused on so-called ΛCDM cosmologies based on the $\Omega_\Lambda - \Omega_m$ contribution to the curvature discussed above.

2. Lecture 2

2.1. *Big Bang Nucleosynthesis*

The standard model[44] of big bang nucleosynthesis (BBN) is based on the relatively simple idea of including an extended nuclear network into a homogeneous and isotropic cosmology. Apart from the input nuclear cross

sections, the theory contains only a single parameter, namely the baryon-to-photon ratio, η. Other factors, such as the uncertainties in reaction rates, and the neutron mean-life can be treated by standard statistical and Monte Carlo techniques[45,46]. The theory then allows one to make predictions (with well-defined uncertainties) of the abundances of the light elements, D, ^{3}He, ^{4}He, and ^{7}Li.

2.1.1. *Theory*

Conditions for the synthesis of the light elements were attained in the early Universe at temperatures $T \gtrsim 1$ MeV. In the early Universe, the energy density was dominated by radiation with

$$\rho = \frac{\pi^2}{30}(2 + \frac{7}{2} + \frac{7}{4}N_\nu)T^4 \tag{16}$$

from the contributions of photons, electrons and positrons, and N_ν neutrino flavors (at higher temperatures, other particle degrees of freedom should be included as well). At these temperatures, weak interaction rates were in equilibrium. In particular, the processes

$$\begin{aligned} n + e^+ &\leftrightarrow p + \bar{\nu}_e \\ n + \nu_e &\leftrightarrow p + e^- \\ n &\leftrightarrow p + e^- + \bar{\nu}_e \end{aligned} \tag{17}$$

fix the ratio of number densities of neutrons to protons. At $T \gg 1$ MeV, $(n/p) \simeq 1$.

The weak interactions do not remain in equilibrium at lower temperatures. Freeze-out occurs when the weak interaction rate, $\Gamma_{wk} \sim G_F^2 T^5$ falls below the expansion rate which is given by the Hubble parameter, $H \sim \sqrt{G_N \rho} \sim T^2/M_P$, where $M_P = 1/\sqrt{G_N} \simeq 1.2 \times 10^{19}$ GeV. The β-interactions in eq. (17) freeze-out at about 0.8 MeV. As the temperature falls and approaches the point where the weak interaction rates are no longer fast enough to maintain equilibrium, the neutron to proton ratio is given approximately by the Boltzmann factor, $(n/p) \simeq e^{-\Delta m/T} \sim 1/6$, where Δm is the neutron-proton mass difference. After freeze-out, free neutron decays drop the ratio slightly to about 1/7 before nucleosynthesis begins.

The nucleosynthesis chain begins with the formation of deuterium by the process, $p + n \rightarrow \mathrm{D} + \gamma$. However, because of the large number of photons relative to nucleons, $\eta^{-1} = n_\gamma/n_B \sim 10^{10}$, deuterium production

is delayed past the point where the temperature has fallen below the deuterium binding energy, $E_B = 2.2$ MeV (the average photon energy in a blackbody is $\bar{E}_\gamma \simeq 2.7T$). This is because there are many photons in the exponential tail of the photon energy distribution with energies $E > E_B$ despite the fact that the temperature or $\bar{E}_\gamma$ is less than E_B. The degree to which deuterium production is delayed can be found by comparing the qualitative expressions for the deuterium production and destruction rates,

$$\begin{aligned} \Gamma_p &\approx n_B \sigma v \\ \Gamma_d &\approx n_\gamma \sigma v e^{-E_B/T} \end{aligned} \tag{18}$$

When the quantity $\eta^{-1}\exp(-E_B/T) \sim 1$, the rate for deuterium destruction ($D + \gamma \rightarrow p + n$) finally falls below the deuterium production rate and the nuclear chain begins at a temperature $T \sim 0.1 MeV$.

The dominant product of big bang nucleosynthesis is ^{4}He and its abundance is very sensitive to the (n/p) ratio

$$Y_p = \frac{2(n/p)}{[1 + (n/p)]} \approx 0.25 \tag{19}$$

i.e., an abundance of close to 25% by mass. Lesser amounts of the other light elements are produced: D and ^{3}He at the level of about 10^{-5} by number, and ^{7}Li at the level of 10^{-10} by number.

The resulting abundances of the light elements[46] are shown in Figure 6, over the range in $\eta_{10} = 10^{10}\eta$ between 1 and 10. The left plot shows the abundance of ^{4}He by mass, Y, and the abundances of the other three isotopes by number. The curves indicate the central predictions from BBN, while the bands correspond to the uncertainty in the predicted abundances based primarily the uncertainty in the input nuclear reactions as computed by Monte Carlo in ref. [46]. This theoretical uncertainty is shown explicitly in the right panel as a function of η_{10}. The dark shaded boxes correspond to the observed abundances of ^{4}He and ^{7}Li and will be discussed below. The dashed boxes correspond to the ranges of the elements consistent with the systematic uncertainties in the observations. The broad band shows a liberal range for η_{10} consistent with the observations. At present, there is a general concordance between the theoretical predictions and the observational data.

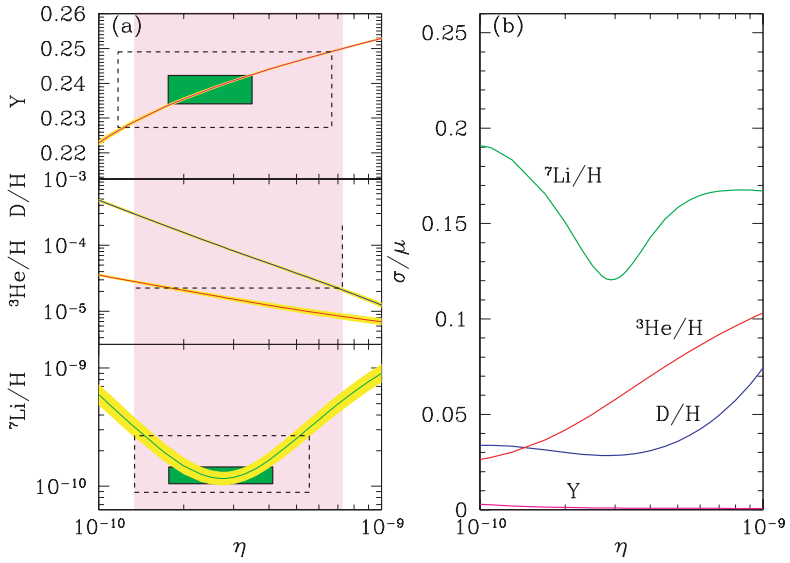

Figure 6. The light element abundances from big bang nucleosynthesis as a function of η_{10}.

2.1.2. *Abundances*

In addition to it BBN production, ^{4}He is made in stars, and thus co-produced with heavy elements. Hence the best sites for determining the primordial ^{4}He abundance are in metal-poor regions of hot, ionized gas in nearby external galaxies (extragalactic HII regions). Helium indeed shows a linear correlation with metallicity in these systems, and the extrapolation to zero metallicity gives the primordial abundance (baryonic mass fraction)[47]

$$Y_p = 0.238 \pm 0.002 \pm 0.005. \tag{20}$$

Here, the first error is statistical and reflects the large sample of systems, whilst the second error is systematic and dominates.

The systematic uncertainties in these observations have not been thoroughly explored to date[48]. In particular, there may be reason to suspect that the above primordial abundance will be increased due to effects such as underlying stellar absorption in the HII regions. We note that other analyses give similar results: $Y_p = 0.244 \pm 0.002 \pm 0.005$ [49] and 0.239 ± 0.002 [50].

The primordial ^{7}Li abundance comes from measurements in the atmospheres of primitive (Population II) stars in the stellar halo of our Galaxy. The ^{7}Li/H abundance is found to be constant for stars with low metallicity, indicating a primordial component, and a recent determination gives

$$\left(\frac{^7\mathrm{Li}}{\mathrm{H}}\right)_p = (1.23 \pm 0.06^{+0.68}_{-0.32}) \times 10^{-10} \ (95\% \ \mathrm{CL}), \tag{21}$$

where the small statistical error is overshadowed by systematic uncertainties[51]. The range (21) may, however, be underestimated, as a recent determination[52] uses a different procedure to determine stellar atmosphere parameters, and gives $^7\mathrm{Li/H}_p = (2.19 \pm 0.28) \times 10^{-10}$. At this stage, it is not possible to determine which method of analysis is more accurate, indicating the likelihood that the upper systematic uncertainty in (21) has been underestimated. Thus, in order to obtain a conservative bound from ^{7}Li, we take the lower bound from (21) and the upper bound from[52], giving

$$9.0 \times 10^{-11} < \left(\frac{^7\mathrm{Li}}{\mathrm{H}}\right)_p < 2.8 \times 10^{-10}. \tag{22}$$

Deuterium is measured in high-redshift QSO absorption line systems via its isotopic shift from hydrogen. In several absorbers of moderate column density (Lyman-limit systems), D has been observed in multiple Lyman transitions[53,54]. Restricting our attention to the three most reliable regions[53], we find a weighted mean of

$$\left(\frac{\mathrm{D}}{\mathrm{H}}\right)_p = (2.9 \pm 0.3) \times 10^{-5}. \tag{23}$$

It should be noted, however, that the χ^2 per degree of freedom is rather poor (~ 3.4), and that the unweighted dispersion of these data is $\sim 0.6 \times 10^{-5}$. This already points to the dominance of systematic effects. Observation of D in systems with higher column density (damped systems) find lower D/H [55], at a level inconsistent with (23), further suggesting that systematic effects dominate the error budget[56]. If all five available observations are used, we would find $\mathrm{D/H} = (2.6 \pm 0.3) \times 10^{-5}$ with an even worse χ^2 per degree of freedom (~ 4.3) and an unweighted dispersion of 0.8.

Because there are no known astrophysical sites for the production of deuterium, all observed D is assumed to be primordial[57]. As a result, any firm determination of a deuterium abundance establishes an upper bound on η which is robust. Thus, the recent measurements of D/H [53] at least provide a lower bound on D/H, $\mathrm{D/H} > 2.1 \times 10^{-5} (2\sigma)$ and hence provide an upper bound to η, $\eta_{10} < 7.3$ and $\Omega_B h^2 < 0.027$.

Helium-3 can be measured through its hyperfine emission in the radio band, and has been observed in HII regions in our Galaxy. These observations find[58] that there are no obvious trends in ^{3}He with metallicity and location in the Galaxy. There is, however, considerable scatter in the data by a factor ~ 2, some of which may be real. Unfortunately, the stellar and Galactic evolution of ^{3}He is not yet sufficiently well understood to confirm whether ^{3}He is increasing or decreasing from its primordial value[59]. Consequently, it is unclear whether the observed ^{3}He abundance represents an upper or lower limit to the primordial value. Therefore, we can not use ^{3}He abundance as a constraint.

By combining the predictions of BBN calculations with the abundances of D, ^{4}He, and ^{7}Li discussed above one can determine the the 95% CL region $4.9 < \eta_{10} < 6.4$, with the peak value occurring at $\eta_{10} = 5.6$. This range corresponds to values of Ω_B between

$$0.018 < \Omega_B h^2 < 0.023 \tag{24}$$

with a central value of $\Omega_B h^2 = 0.020$.

If we were to use only the deuterium abundance from Eq. 23, one obtains the 95% CL range $5.3 < \eta_{10} < 7.3$, with the peak value occurring at $\eta_{10} = 5.9$. This range corresponds to values of Ω_B between

$$0.019 < \Omega_B h^2 < 0.027 \tag{25}$$

with a central value of $\Omega_B h^2 = 0.021$. As one can see from a comparison with Table 1, these values are in excellent agreement with determinations from the CMB.

2.2. *Candidates*

2.2.1. *Baryons*

Accepting the dark matter hypothesis, the first choice for a candidate should be something we know to exist, baryons. Though baryonic dark matter can not be the whole story if $\Omega_m > 0.1$, the identity of the dark matter in galactic halos, which appear to contribute at the level of $\Omega \sim 0.05$, remains an important question needing to be resolved. A baryon density of this magnitude is not excluded by nucleosynthesis. Indeed we know some of the baryons are dark since $\Omega \lesssim 0.01$ in the disk of the galaxy.

It is interesting to note that until recently, there seemed to be some difficulty in reconciling the baryon budget of the Universe. By counting the visible contribution to Ω in stellar populations and the X-ray producing hot

gas, Persic and Salucci[60] found only $\Omega_{\rm vis} \simeq 0.003$. A subsequent accounting by Fukugita, Hogan and Peebles[61] found slightly more ($\Omega \sim 0.02$) by including the contribution from plasmas in groups and clusters. At high redshift on the other hand, all of the baryons can be accounted for. The observed opacity of the Ly α forest in QSO absorption spectra requires a large baryon density consistent with the determinations by the CMB and BBN[62].

In galactic halos, however, it is quite difficult to hide large amounts of baryonic matter[63]. Sites for halo baryons that have been discussed include Hydrogen (frozen, cold or hot gas), low mass stars/Jupiters, remnants of massive stars such as white dwarfs, neutron stars or black holes. In almost every case, a serious theoretical or observational problem is encountered.

2.2.1.1 Hydrogen

A halo predominately made of hydrogen (with a primordial admixture of ^{4}He) is perhaps the simplest possibility. Hydrogen may however be present in a condensed snow-ball like state or in the form of gas. Aside from the obvious question of how do these snowballs get made, it is possible to show that their existence today requires them to be so large as to be gravitationally bound[63].

Assuming that these objects are electrostatically bound, the average density of solid hydrogen is $\rho_s = 0.07$ g cm^{-3} and the binding energy per molecule is about 1 eV. Given that the average velocity of a snowball is $v \sim 250$ kms^{-1}, corresponding to a kinetic energy $E_k \sim 600$ eV, snowballs must be collisionless in order to survive. Requiring that the collision rate $\Gamma_c = n_s \sigma v$ be less than ${t_u}^{-1}$ (t_u is the age of the halo $\simeq$ age of the Universe) with $n_s = \rho_H / m_s$ and $\sigma = \pi {r_s}^2$ one finds $r_s \gtrsim 2$ cm and $m_s \gtrsim 1$ g, assuming a halo density $\rho_H = 1.7 \times 10^{-26}$ g cm^{-3} (corresponding to $10^{12} M_\odot$ in a radius of 100 kpc). However, collisionless snowballs also require that their formation occur when the overall density $\rho = \rho_H$. In this case, snowballs could not have formed later than a redshift $(1 + z) = 3.5$ or when the microwave background temperature was 9.5K. At this temperature, there is no equilibrium between the gaseous and condensed state and the snowballs would sublimate. For a snowball to survive, $r_s > 10^{16}$ cm is required making this no longer an electrostatically bound object.

If snowballs sublimate, then we can consider the possibility of a halo composed of cold hydrogen gas. Because the collapse time-scale for the halo ($< 10^9$ yrs) is much less than the age of the galaxy, the gas must be

in hydrostatic equilibrium. Combining the equation of state

$$P(r) = (2\rho(r)/m_p)kT \tag{26}$$

where m_p is the proton mass, with

$$dP(r)/dr = -\frac{GM(r)\rho(r)}{r^2} \tag{27}$$

one can solve for the equilibrium temperature

$$T = \frac{Gm_pM(r)}{4kr} \simeq 1.3 \times 10^6 K \tag{28}$$

This is hot gas. As discussed earlier, hot gas is observed through X-ray emission. It is easy to show that an entire halo of hot gas would conflict severely with observations. Cooling of course may occur, but at the expense of star formation.

2.2.1.2 Jupiter-like objects

A very popular candidate for baryonic dark matter is a very low mass star or JLO. These are objects with a mass $m < m_o = 0.08M_\odot$, the mass necessary to commence nuclear burning. Presumably there is a minimum mass[64] $m > m_{min} = (0.004 - 0.007)M_\odot$ based on fragmentation, but the exact value is very uncertain. The contribution of these objects to the dark matter in the halo depends on how much mass can one put between m_{min} and m_o and depends on the initial mass function (IMF) in the halo.

An IMF is the number of stars formed per unit volume per unit mass and can be parameterized as

$$\phi = Am^{-(1+x)} \tag{29}$$

In this parametrization, the Salpeter mass function corresponds to x = 1.35. Because stars are not observed with $m < m_o$, some assumptions about the IMF for low masses must be made. An example of the observed[65] IMF in the solar neighborhood is shown in Fig. 7.

It is possible to use infrared observations[66] to place a lower limit on the slope, x, of the IMF in the halo of galaxies by comparing a mass-to-light ratio defined by

$$Q = (\rho_m/\rho_L)\, L_\odot/M_\odot \tag{30}$$

where the total mass density in JLO's and low mass stars is given by

$$\rho_m = \int_{m_{min}}^{m_G} m\phi dm \tag{31}$$

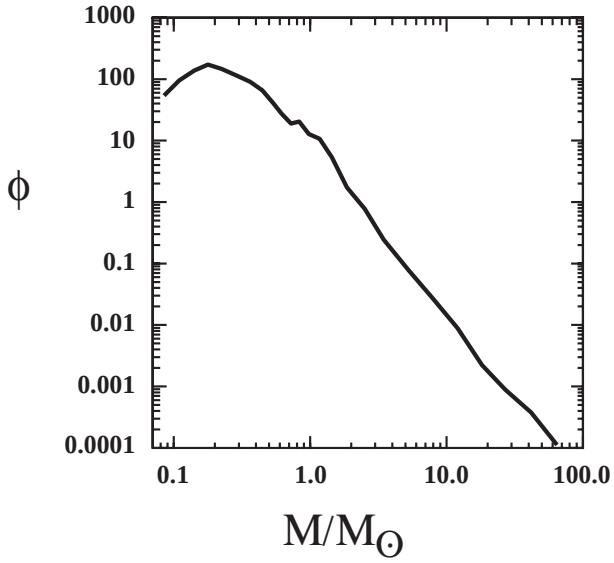

Figure 7. The IMF in the solar neighborhood[65].

where $m_G = 0.75 M_\odot$ is the mass of a giant. The luminosity density given by such a stellar distribution is

$$\rho_L = \int_{m_o}^{m_G} L\phi dm + \rho_G \tag{32}$$

where $L(m)$ is the luminosity of a star of mass m. ρ_G is the contribution to the luminosity density due to giant stars. The observed[66] lower limits on Q translate to a limit[63] on x

$$x > 1.7 \tag{33}$$

with a weak dependence of m_{min}.

Unfortunately, one can not use Eq. (33) to exclude JLO's since we do not observe an IMF in the halo and it may be different from that in the disk. One can however make a comparison with existing observations, none of which show such a steep slope at low masses. Indeed, most observations leading to a determination of the IMF (such as the one shown in Fig. 7) show a turn over (or negative slope). To fully answer the questions regarding JLO's in the halo, one needs a better understanding of star formation and the IMF. For now, postulating the existence of a large fraction of JLO's in halo is rather ad-hoc.

Despite the theoretical arguments against them, JLO's or massive compact halo objects (MACHOs) are candidates which are testable by the gravitational microlensing of stars in a neighboring galaxy such as the LMC[67]. By observing millions of stars and examining their intensity as a function of time, it is possible to determine the presence of dark objects in our halo. It is expected that during a lensing event, a star in the LMC will have its intensity rise in an achromatic fashion over a period $\delta t \sim 3\ \sqrt{M/.001 M_\odot}$ days. Indeed, microlensing candidates have been found[68]. For low mass objects, those with $M < 0.1 M_\odot$, it appears however that the halo fraction of MACHOs is very small. The relative amount of machos in the halo is typically expressed in terms of an optical depth. A halo consisting 100% of machos would have an optical depth of $\tau \sim 5 \times 10^{-7}$. The most recent results of the MACHO collaboration[69] indicate that $\tau = 12^{+4}_{-3} \times 10^{-8}$, corresponding to a macho halo fraction of about 20% with a 95% CL range of 8 – 50% based on 13 – 17 events. They also exclude a 100% macho halo at the 95% CL. The typical macho mass falls in the range 0.15 – 0.9 $M_\odot$. The EROS collaboration has set even stronger limits having observed 5 events toward the LMC and 4 toward the SMC[70]. The observed optical depth from EROS1 is $\tau = 4^{+10}_{-4} \times 10^{-8}$ and from EROS2 $\tau = 6^{+5}_{-3} \times 10^{-8}$. They have excluded low mass objects ($M < 0.1 M_\odot$) to make up less than 10% of the halo and objects with $2 \times 10^{-7} M_\odot < M < 1 M_\odot$ to be less than 25% of the halo at the 95% CL.

2.2.1.3 Remnants of Massive Stars

Next one should possibility that the halo is made up of the dead stellar remnants of stars whose initial masses were $M > 1 M_\odot$. Briefly, the problem which arises in this context is that since at least 40% of the stars initial mass is ejected, and most of this mass is in the form of heavy elements, a large population of these objects would contaminate the disk and prevent the existence of extremely low metallicity objects ($Z \sim 10^{-5}$) which have been observed. Thus either dust (from ejecta) or dead remnants would be expected to produce too large a metallicity[63,71]. Clearly star formation is a very inefficient mechanism for producing dark matter. Many generations of stars would would be required to cycle through their lifetimes to continually trap more matter in remnants.

This question has been studied in more detail[72]. By allowing a variable star formation rate, and allowing a great deal of flexibility in the IMF, a search for a consistent set of parameters so that the halo could be described primarily in terms of dead remnants (in this case white dwarfs) was per-

formed. While a consistent set of chemical evolution parameters can be found, there is no sensible theory to support this choice. In such a model however, the dark matter is in the form of white dwarfs and the remaining gas is is heavily contaminated by Carbon and Nitrogen[73]. Though it is not excluded, it is hard to understand this corner of parameter space as being realistic.

2.2.1.4 Black Holes

There are several possibilities for black holes as the dark matter in halos. If the black holes are primordial[74] which have presumably formed before nucleosynthesis, they should not be counted as baryonic dark matter and therefore do not enter into the present discussion. If the black holes are formed as the final stage of star's history and its formation was preceded by mass loss or a supernovae, then the previous discussion on remnants of massive stars applies here as well. However, it is also possible that the black halos were formed directly from very massive stars ($m > 100 M_{\odot}$?) through gravitational instability with no mass loss[75]. Though there are limits due to overheating the disk[76] and stellar systems[77]. In this case I know of no argument preventing a sufficiently large population of massive black holes as baryonic dark matter (Of course, now the IMF must have $m_{min} \gtrsim 100 M_{\odot}$.)

2.2.2. *Neutrinos*

Light neutrinos ($m \leq 30eV$) are a long-time standard when it comes to non-baryonic dark matter[78]. Light neutrinos produce structure on large scales, and the natural (minimal) scale for structure clustering is given in Eq. (15). Hence neutrinos offer the natural possibility for large scale structures[79,80] including filaments and voids. Light neutrinos are, however, ruled out as a dominant form of dark matter because they produce too much large scale structure[81]. Because the smallest non-linear structures have mass scale M_J and the typical galactic mass scale is $\simeq 10^{12} M_{\odot}$, galaxies must fragment out of the larger pancake-like objects. The problem with such a scenario is that galaxies form late[80,82] ($z \leq 1$) whereas quasars and galaxies are seen out to redshifts $z \gtrsim 6$.

In the standard model, the absence of a right-handed neutrino state precludes the existence of a neutrino mass (unless one includes non-renormalizable lepton number violating interactions such HHLL). By adding a right-handed state ν_R, it is possible to generate a Dirac mass for

the neutrino, $m_\nu = h_\nu v/\sqrt{2}$, as is the case for the charged lepton masses, where h_ν is the neutrino Yukawa coupling constant, and v is the Higgs expectation value. It is also possible to generate a Majorana mass for the neutrino when in addition to the Dirac mass term, $m_\nu \bar{\nu_R} \nu_L$, a term $M \nu_R \nu_R$ is included. If $M \gg m_\nu$, the see-saw mechanism produces two mass eigenstates given by $m_{\nu_1} \sim m_\nu^2/M$ which is very light, and $m_{\nu_2} \sim M$ which is heavy. The state ν_1 is a potential hot dark matter candidate as ν_2 is in general not stable.

The simplicity of the standard big bang model allows one to compute in a straightforward manner the relic density of any stable particle if that particle was once in thermal equilibrium with the thermal radiation bath. At early times, neutrinos were kept in thermal equilibrium by their weak interactions with electrons and positrons. As we saw in the case of the β-interaction used in BBN, one can estimate the thermally averaged low-energy weak interaction scattering cross section

$$\langle \sigma v \rangle \sim g^4 T^2 / m_W^4 \tag{34}$$

for $T \ll m_W$. Recalling that the number density scales as $n \propto T^3$, we can compare the weak interaction rate $\Gamma \sim n \langle \sigma v \rangle$, with the expansion rate given by eqs. (6) with

$$\rho = \left(\sum_B g_B + \frac{7}{8} \sum_F g_F \right) \frac{\pi^2}{30} T^4 \equiv \frac{\pi^2}{30} N(T) T^4 \tag{35}$$

Neutrinos will be in equilibrium when $\Gamma_{\rm wk} > H$ or

$$T^3 > \sqrt{8\pi^3 N/90}\ m_W^4/M_P \tag{36}$$

where $M_P = G_N^{-1/2} = 1.22 \times 10^{19}$ GeV is the Planck mass. For $N = 43/4$ (accounting for photons, electrons, positrons and three neutrino flavors) we see that equilibrium is maintained at temperatures greater than $\mathcal{O}(1)$ MeV (for a more accurate calculation see [83]).

The decoupling scale of $\mathcal{O}(1)$ MeV has an important consequence on the final relic density of massive neutrinos. Neutrinos more massive than 1 MeV will begin to annihilate prior to decoupling, and while in equilibrium, their number density will become exponentially suppressed. Lighter neutrinos decouple as radiation on the other hand, and hence do not experience the suppression due to annihilation. Therefore, the calculations of the number density of light ($m_\nu \lesssim 1$ MeV) and heavy ($m_\nu \gtrsim 1$ MeV) neutrinos differ substantially.

The number of density of light neutrinos with $m_\nu \lesssim 1$ MeV can be expressed at late times as

$$\rho_\nu = m_\nu Y_\nu n_\gamma \tag{37}$$

where $Y_\nu = n_\nu/n_\gamma$ is the density of ν's relative to the density of photons, which today is 411 photons per cm^3. It is easy to show that in an adiabatically expanding universe $Y_\nu = 3/11$. This suppression is a result of the e^+e^- annihilation which occurs after neutrino decoupling and heats the photon bath relative to the neutrinos. In order to obtain an age of the Universe, $t > 12$ Gyr, one requires that the matter component is constrained by

$$\Omega h^2 \leq 0.3. \tag{38}$$

From this one finds the strong constraint (upper bound) on Majorana neutrino masses[84]:

$$m_{\rm tot} = \sum_\nu m_\nu \lesssim 28{\rm eV}. \tag{39}$$

where the sum runs over neutrino mass eigenstates. The limit for Dirac neutrinos depends on the interactions of the right-handed states (see discussion below). Given the discussion of the CMB results in the previous section, one could make a case that the limit on Ωh^2 should be reduced by a factor of 2, which would translate in to a limit of 14 eV on the sum of the light neutrino masses. As one can see, even very small neutrino masses of order 1 eV, may contribute substantially to the overall relic density. The limit (39) and the corresponding initial rise in $\Omega_\nu h^2$ as a function of m_ν is displayed in the Figure 8 (the low mass end with $m_\nu \lesssim 1$ MeV).

Combining the rapidly improving data on key cosmological parameters with the better statistics from large redshift surveys has made it possible to go a step forward along this path. It is now possible to set stringent limits on the light neutrino mass density $\Omega_\nu h^2$, and hence on the neutrino mass based on the power spectrum of the Ly α forest[86], $m_{\rm tot} < 5.5$ eV, and the limit is even stronger if the total matter density, Ω_m is less than 0.5. Adding additional observation constraints from the CMB and galaxy clusters drops this limit[87] to 2.4 eV. This limit has recently been improved by the 2dF Galaxy redshift[88] survey by comparing the derived power spectrum of fluctuations with structure formation models. Focussing on the the presently favoured ΛCDM model, the neutrino mass bound becomes $m_{\rm tot} < 1.8$ eV for $\Omega_m < 0.5$. When even more constraints such as HST

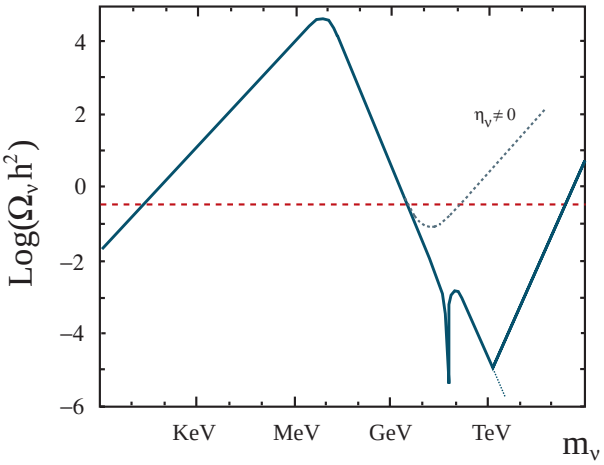

Figure 8. Summary plot[85] of the relic density of Dirac neutrinos (solid) including a possible neutrino asymmetry of $\eta_\nu = 5 \times 10^{-11}$ (dotted).

Key project data, supernovae type Ia data, and BBN are included[89] the limit can be pushed to $m_{\rm tot} < 0.3$ eV.

The calculation of the relic density for neutrinos more massive than ~ 1 MeV, is substantially more involved. The relic density is now determined by the freeze-out of neutrino annihilations which occur at $T \lesssim m_\nu$, after annihilations have begun to seriously reduce their number density[90]. The annihilation rate is given by

$$\Gamma_{ann} = \langle \sigma v \rangle_{ann} n_\nu \sim \frac{m_\nu^2}{m_Z^4} (m_\nu T)^{3/2} e^{-m_\nu/T} \tag{40}$$

where we have assumed, for example, that the annihilation cross section is dominated by $\nu\bar{\nu} \to f\bar{f}$ via Z-boson exchange[a] and $\langle \sigma v \rangle_{ann} \sim m_\nu^2/m_Z^4$. When the annihilation rate becomes slower than the expansion rate of the Universe the annihilations freeze out and the relative abundance of neutrinos becomes fixed. For particles which annihilate through approximate weak scale interactions, this occurs when $T \sim m_\chi/20$. The number density

[a]While this is approximately true for Dirac neutrinos, the annihilation cross section of Majorana neutrinos is p-wave suppressed and is proportional of the final state fermion masses rather than m_ν.

of neutrinos is tracked by a Boltzmann-like equation,

$$\frac{dn}{dt} = -3\frac{\dot{R}}{R}n - \langle\sigma v\rangle(n^2 - n_0^2) \tag{41}$$

where n_0 is the equilibrium number density of neutralinos. By defining the quantity $f = n/T^3$, we can rewrite this equation in terms of x, as

$$\frac{df}{dx} = m_\nu \left(\frac{8\pi^3}{90}G_N N\right)^{1/2}(f^2 - f_0^2) \tag{42}$$

The solution to this equation at late times (small x) yields a constant value of f, so that $n \propto T^3$.

Roughly, the solution to the Boltzmann equation goes as $Y_\nu \sim f \sim (m\langle\sigma v\rangle_{ann})^{-1}$ and hence $\Omega_\nu h^2 \sim \langle\sigma v\rangle_{ann}{}^{-1}$, so that parametrically $\Omega_\nu h^2 \sim 1/m_\nu^2$. As a result, the constraint (38) now leads to a *lower* bound[90,91,92] on the neutrino mass, of about $m_\nu \gtrsim 3 - 7$ GeV, depending on whether it is a Dirac or Majorana neutrino. This bound and the corresponding downward trend $\Omega_\nu h^2 \sim 1/m_\nu^2$ can again be seen in Figure 8. The result of a more detailed calculation is shown in Figure 9 [92] for the case of a Dirac neutrino. The two curves show the slight sensitivity on the temperature scale associated with the quark-hadron transition. The result for a Majorana mass neutrino is qualitatively similar. Indeed, any particle with roughly weak scale cross-sections will tend to give an interesting value of $\Omega h^2 \sim 1$.

The deep drop in $\Omega_\nu h^2$, visible in Figure 8 at around $m_\nu = M_Z/2$, is due to a very strong annihilation cross section at Z-boson pole. For yet higher neutrino masses the Z-annihilation channel cross section drops as $\sim 1/m_\nu^2$, leading to a brief period of an increasing trend in $\Omega_\nu h^2$. However, for $m_\nu \gtrsim m_W$ the cross section regains its parametric form $\langle\sigma v\rangle_{ann} \sim m_\nu^2$ due to the opening up of a new annihilation channel to W-boson pairs[93], and the density drops again as $\Omega_\nu h^2 \sim 1/m_\nu^2$. The tree level W-channel cross section breaks the unitarity at around $\mathcal{O}$(few) TeV [94] however, and the full cross section must be bound by the unitarity limit[95]. This behaves again as $1/m_\nu^2$, whereby $\Omega_\nu h^2$ has to start increasing again, until it becomes too large again at 200-400 TeV [95,94] (or perhaps somewhat earlier as the weak interactions become strong at the unitarity breaking scale).

If neutrinos are Dirac particles, and have a nonzero asymmetry the relic density could be governed by the asymmetry rather than by the annihilation cross section. Indeed, it is easy to see that the neutrino mass density corresponding to the asymmetry $\eta_\nu \equiv (n_\nu - n_{\bar{\nu}})/n_\gamma$ is given by[96]

$$\rho = m_\nu \eta_\nu n_\gamma, \tag{43}$$

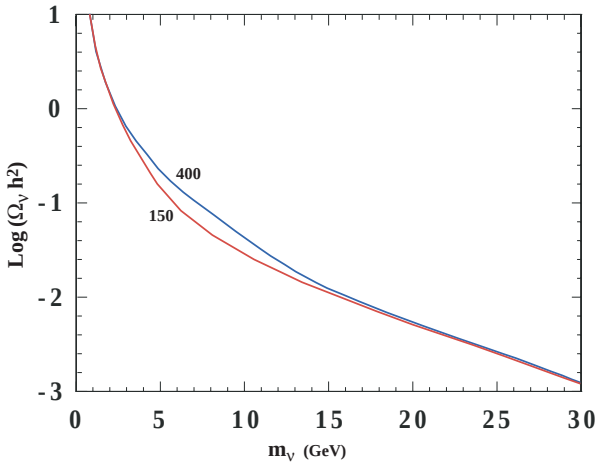

Figure 9. The relic density of heavy Dirac neutrinos due to annihilations[92]. The curves are labeled by the assumed quark-hadron phase transition temperature in MeV.

which implies

$$\Omega_\nu h^2 \simeq 0.004\,\eta_{\nu 10}\,(m_\nu/\mathrm{GeV}). \tag{44}$$

where $\eta_{\nu 10} \equiv 10^{10}\eta_\nu$. The behaviour of the energy density of neutrinos with an asymmetry is shown by the dotted line in the Figure 8. At low m_ν, the mass density is dominated by the symmetric, relic abundance of both neutrinos and antineutrinos which have already frozen out. At higher values of m_ν, the annihilations suppress the symmetric part of the relic density until $\Omega_\nu h^2$ eventually becomes dominated by the linearly increasing asymmetric contribution. In the figure, we have assumed an asymmetry of $\eta_\nu \sim 5 \times 10^{-11}$ for neutrinos with standard weak interaction strength. In this case, $\Omega_\nu h^2$ begins to rise when $m_\nu \gtrsim 20$ GeV. Obviously, the bound (38) is saturated for $m_\nu = 75\,\mathrm{GeV}/\eta_{\nu 10}$.

Based on the leptonic and invisible width of the Z boson, experiments at LEP have determined that the number of neutrinos is $N_\nu = 2.9841 \pm 0.0083$ [97]. Conversely, any new physics must fit within these brackets, and thus LEP excludes additional neutrinos (with standard weak interactions) with masses $m_\nu \lesssim 45$ GeV. Combined with the limits displayed in Figures 8 and 9, we see that the mass density of ordinary heavy neutrinos is bound to be very small, $\Omega_\nu h^2 < 0.001$ for masses $m_\nu > 45$ GeV up to $m_\nu \sim \mathcal{O}(100)$ TeV. Lab constraints for Dirac neutrinos are

available[98], excluding neutrinos with masses between 10 GeV and 4.7 TeV. This is significant, since it precludes the possibility of neutrino dark matter based on an asymmetry between ν and $\bar{\nu}$ [96]. Majorana neutrinos are excluded as *dark matter* since ${\Omega_\nu h_o}^2 < 0.001$ for $m_\nu > 45$ GeV and are thus cosmologically uninteresting.

A bound on neutrino masses even stronger than Eqn. (39) can be obtained from the recent observations of active-active mixing in both solar- and atmospheric neutrino experiments. The inferred evidence for $\nu_\mu - \nu_\tau$ and $\nu_e - \nu_{\mu,\tau}$ mixings are on the scales $m_\nu^2 \sim 1 - 10 \times 10^{-5}$ and $m_\nu^2 \sim 2 - 5 \times 10^{-3}$. When combined with the upper bound on the electron-like neutrino mass $m_\nu < 2.8$ eV [99], and the LEP-limit on the number of neutrino species, one finds the constraint on the sum of neutrino masses:

$$0.05 \text{ eV} \lesssim m_{\text{tot}} \lesssim 8.4 \text{ eV}. \tag{45}$$

Conversely, the experimental and observational data then implies that the cosmological energy density of all light, weakly interacting neutrinos can be restricted to the range

$$0.0005 \lesssim \Omega_\nu h^2 \lesssim 0.09. \tag{46}$$

Interestingly there is now also a lower bound due to the fact that at least one of the neutrino masses has to be larger than the scale $m^2 \sim 10^{-3}$ eV^2 set by the atmospheric neutrino data. Combined with the results on relic mass density of neutrinos and the LEP limits, the bound (46) implies that the ordinary weakly interacting neutrinos, once the standard dark matter candidate[78], can be ruled out completely as a dominant component of the dark matter.

If instead, we consider right-handed neutrinos, we have new possibilities. Right-handed interactions are necessarily weaker than standard left-handed interactions implying that right-handed neutrinos decouple early and today are at a reduced temperature relative to ν_L [100]

$$(\frac{T_\chi}{T_\gamma})^3 = \frac{43}{4N(T_d)} \tag{47}$$

As such, for $T_{dR} \gg 1$ MeV, $n_{\nu_R}/n_{\nu_L} = (T_{\nu_R}/T_{\nu_L})^3 \ll 1$. Thus the abundance of right-handed neutrinos can be written as

$$Y_{\nu_R} = \frac{n_{\nu_R}}{n_\gamma} = (\frac{3}{11})(\frac{T_{\nu_R}}{T_{\nu_L}})^3 \ll \frac{3}{11} \tag{48}$$

In this case, the previous bound (39) on neutrino masses is weakened. For a suitably large scale for the right-handed interactions, right-handed neutrino

masses may be as large as a few keV [101]. Such neutrinos make excellent warm dark matter candidates, albeit the viable mass range for galaxy formation is quite restricted[102].

2.2.3. *Axions*

Due to space limitations, the discussion of this candidate will be very brief. Axions are pseudo-Goldstone bosons which arise in solving the strong CP problem[103,104] via a global U(1) Peccei-Quinn symmetry. The invisible axion[104] is associated with the flat direction of the spontaneously broken PQ symmetry. Because the PQ symmetry is also explicitly broken (the CP violating $\theta F\widetilde{F}$ coupling is not PQ invariant) the axion picks up a small mass similar to pion picking up a mass when chiral symmetry is broken. We can expect that $m_a \sim m_\pi f_\pi / f_a$ where f_a, the axion decay constant, is the vacuum expectation value of the PQ current and can be taken to be quite large. If we write the axion field as $a = f_a\theta$, near the minimum, the potential produced by QCD instanton effects looks like $V \sim m_a^2\theta^2 f_a^2$. The axion equations of motion lead to a relatively stable oscillating solution. The energy density stored in the oscillations exceeds the critical density[105] unless $f_a \lesssim 10^{12}$ GeV.

Axions may also be emitted stars and supernova[106]. In supernovae, axions are produced via nucleon-nucleon bremsstrahlung with a coupling $g_A N \propto m_N/f_a$. As was noted above the cosmological density limit requires $f_a \lesssim 10^{12}$ GeV. Axion emission from red giants imply[107] $f_a \gtrsim 10^{10}$ GeV (though this limit depends on an adjustable axion-electron coupling), the supernova limit requires[108] $f_a \gtrsim 2 \times 10^{11}$ GeV for naive quark model couplings of the axion to nucleons. Thus only a narrow window exists for the axion as a viable dark matter candidate.

3. Lecture 3: Supersymmetric Dark Matter

Although there are many reasons for considering supersymmetry as a candidate extension to the standard model of strong, weak and electromagnetic interactions[109], one of the most compelling is its role in understanding the hierarchy problem[110] namely, why/how is $m_W \ll M_P$. One might think naively that it would be sufficient to set $m_W \ll M_P$ by hand. However, radiative corrections tend to destroy this hierarchy. For example, one-loop diagrams generate

$$\delta m_W^2 = \mathcal{O}\left(\frac{\alpha}{\pi}\right)\ \Lambda^2 \gg m_W^2 \tag{49}$$

where Λ is a cut-off representing the appearance of new physics, and the inequality in (49) applies if $\Lambda \sim 10^3$ TeV, and even more so if $\Lambda \sim m_{GUT} \sim 10^{16}$ GeV or $\sim M_P \sim 10^{19}$ GeV. If the radiative corrections to a physical quantity are much larger than its measured values, obtaining the latter requires strong cancellations, which in general require fine tuning of the bare input parameters. However, the necessary cancellations are natural in supersymmetry, where one has equal numbers of bosons and fermions with equal couplings, so that (49) is replaced by

$$\delta m_W^2 = \mathcal{O}\left(\frac{\alpha}{\pi}\right) \ |m_B^2 - m_F^2| \ . \tag{50}$$

The residual radiative correction is naturally small if $|m_B^2 - m_F^2| \lesssim 1$ TeV^2.

In order to justify the absence of interactions which can be responsible for extremely rapid proton decay, it is common in the minimal supersymmetric standard model (MSSM) to assume the conservation of R-parity. If R-parity, which distinguishes between "normal" matter and the supersymmetric partners and can be defined in terms of baryon, lepton and spin as $R = (-1)^{3B+L+2S}$, is unbroken, there is at least one supersymmetric particle (the lightest supersymmetric particle or LSP) which must be stable. Thus, the minimal model contains the fewest number of new particles and interactions necessary to make a consistent theory.

There are very strong constraints, however, forbidding the existence of stable or long lived particles which are not color and electrically neutral[111]. Strong and electromagnetically interacting LSPs would become bound with normal matter forming anomalously heavy isotopes. Indeed, there are very strong upper limits on the abundances, relative to hydrogen, of nuclear isotopes[112], $n/n_H \lesssim 10^{-15}$ to 10^{-29} for 1 GeV $\lesssim m \lesssim 1$ TeV. A strongly interacting stable relic is expected to have an abundance $n/n_H \lesssim 10^{-10}$ with a higher abundance for charged particles.

There are relatively few supersymmetric candidates which are not colored and are electrically neutral. The sneutrino[113] is one possibility, but in the MSSM, it has been excluded as a dark matter candidate by direct[98] and indirect[114] searches. In fact, one can set an accelerator based limit on the sneutrino mass from neutrino counting, $m_{\tilde{\nu}} \gtrsim 44.7$ GeV [115]. In this case, the direct relic searches in underground low-background experiments require $m_{\tilde{\nu}} \gtrsim 20$ TeV [98]. Another possibility is the gravitino which is probably the most difficult to exclude. I will concentrate on the remaining possibility in the MSSM, namely the neutralinos.

3.1. *Parameters*

The most general version of the MSSM, despite its minimality in particles and interactions contains well over a hundred new parameters. The study of such a model would be untenable were it not for some (well motivated) assumptions. These have to do with the parameters associated with supersymmetry breaking. It is often assumed that, at some unification scale, all of the gaugino masses receive a common mass, $m_{1/2}$. The gaugino masses at the weak scale are determined by running a set of renormalization group equations. Similarly, one often assumes that all scalars receive a common mass, m_0, at the GUT scale. These too are run down to the weak scale. The remaining parameters of importance involve the Higgs sector. There is the Higgs mixing mass parameter, μ, and since there are two Higgs doublets in the MSSM, there are two vacuum expectation values. One combination of these is related to the Z mass, and therefore is not a free parameter, while the other combination, the ratio of the two vevs, $\tan\beta$, is free.

If the supersymmetry breaking Higgs soft masses are also unified at the GUT scale (and take the common value m_0), then μ and the physical Higgs masses at the weak scale are determined by electroweak vacuum conditions (μ is determined up to a sign). This scenario is often referred to as the constrained MSSM or CMSSM. Once these parameters are set, the entire spectrum of sparticle masses at the weak scale can be calculated[b]. In Fig. 10, an example of the running of the mass parameters in the CMSSM is shown. Here, we have chosen $m_{1/2} = 250$ GeV, $m_0 = 100$ GeV, $\tan\beta = 3$, $A_0 = 0$, and $\mu < 0$. Indeed, it is rather amazing that from so few input parameters, all of the masses of the supersymmetric particles can be determined. The characteristic features that one sees in the figure, are for example, that the colored sparticles are typically the heaviest in the spectrum. This is due to the large positive correction to the masses due to α_3 in the RGE's. Also, one finds that the $\widetilde{B}$ (the partner of the $U(1)_Y$ gauge boson), is typically the lightest sparticle. But most importantly, notice that one of the Higgs mass^2, goes negative triggering electroweak symmetry breaking[116]. (The negative sign in the figure refers to the sign of the mass^2, even though it is the mass of the sparticles which are depicted.)

[b]There are in fact, additional parameters: the supersymmetry-breaking tri-linear masses A (also assumed to be unified at the GUT scale) as well as two CP violating phases θ_μ and θ_A.

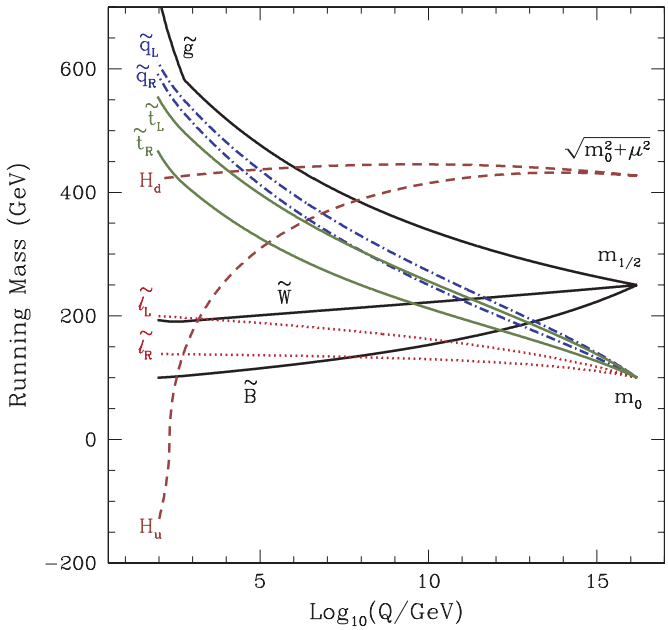

Figure 10. RG evolution of the mass parameters in the CMSSM.

3.2. *Neutralinos*

There are four neutralinos, each of which is a linear combination of the $R = -1$ neutral fermions[111]: the wino $\tilde{W}^3$, the partner of the 3rd component of the $SU(2)_L$ gauge boson; the bino, $\tilde{B}$; and the two neutral Higgsinos, $\tilde{H}_1$ and $\tilde{H}_2$. Assuming gaugino mass universality at the GUT scale, the identity and mass of the LSP are determined by the gaugino mass $m_{1/2}$, μ, and $\tan\beta$. In general, neutralinos can be expressed as a linear combination

$$\chi = \alpha\tilde{B} + \beta\tilde{W}^3 + \gamma\tilde{H}_1 + \delta\tilde{H}_2 \tag{51}$$

The solution for the coefficients α, β, γ and δ for neutralinos that make up the LSP can be found by diagonalizing the mass matrix

$$(\tilde{W}^3, \tilde{B}, \tilde{H}_1^0, \tilde{H}_2^0) \begin{pmatrix} M_2 & 0 & \frac{-g_2 v_1}{\sqrt{2}} & \frac{g_2 v_2}{\sqrt{2}} \\ 0 & M_1 & \frac{g_1 v_1}{\sqrt{2}} & \frac{-g_1 v_2}{\sqrt{2}} \\ \frac{-g_2 v_1}{\sqrt{2}} & \frac{g_1 v_1}{\sqrt{2}} & 0 & -\mu \\ \frac{g_2 v_2}{\sqrt{2}} & \frac{-g_1 v_2}{\sqrt{2}} & -\mu & 0 \end{pmatrix} \begin{pmatrix} \tilde{W}^3 \\ \tilde{B} \\ \tilde{H}_1^0 \\ \tilde{H}_2^0 \end{pmatrix} \tag{52}$$

where $M_1(M_2)$ is a soft supersymmetry breaking term giving mass to the U(1) (SU(2)) gaugino(s). In a unified theory $M_1 = M_2 = m_{1/2}$ at the unification scale (at the weak scale, $M_1 \simeq \frac{5}{3}\frac{\alpha_1}{\alpha_2}M_2$). As one can see, the coefficients α, β, γ, and δ depend only on $m_{1/2}$, μ, and $\tan\beta$.

In Figure 11 [117], regions in the M_2, μ plane with $\tan\beta = 2$ are shown in which the LSP is one of several nearly pure states, the photino, $\tilde{\gamma}$, the bino, $\tilde{B}$, a symmetric combination of the Higgsinos, $\tilde{H}_{(12)}$, or the Higgsino, $\tilde{S} = \sin\beta\tilde{H}_1 + \cos\beta\tilde{H}_2$. The dashed lines show the LSP mass contours. The cross hatched regions correspond to parameters giving a chargino $(\tilde{W}^{\pm}, \tilde{H}^{\pm})$ state with mass $m_{\tilde{\chi}} \leq 45GeV$ and as such are excluded by LEP[118]. This constraint has been extended by LEP[119] and is shown by the light shaded region and corresponds to regions where the chargino mass is $\lesssim 103.5$ GeV. The newer limit does not extend deep into the Higgsino region because of the degeneracy between the chargino and neutralino. Notice that the parameter space is dominated by the $\tilde{B}$ or $\tilde{H}_{12}$ pure states and that the photino only occupies a small fraction of the parameter space, as does the Higgsino combination $\tilde{S}$. Both of these light states are experimentally excluded.

3.3. *The Relic Density*

The relic abundance of LSP's is determined by solving the Boltzmann equation for the LSP number density in an expanding Universe. The technique[92] used is similar to that for computing the relic abundance of massive neutrinos[90]. The relic density depends on additional parameters in the MSSM beyond $m_{1/2}, \mu$, and $\tan\beta$. These include the sfermion masses, $m_{\tilde{f}}$ and the Higgs pseudo-scalar mass, m_A, derived from m_0 (and $m_{1/2}$). To determine the relic density it is necessary to obtain the general annihilation cross-section for neutralinos. In much of the parameter space of interest, the LSP is a bino and the annihilation proceeds mainly through sfermion exchange. Because of the p-wave suppression associated with Majorana fermions, the s-wave part of the annihilation cross-section is suppressed by the outgoing fermion masses. This means that it is necessary to expand the cross-section to include p-wave corrections which can be expressed as a term proportional to the temperature if neutralinos are in equilibrium. Unless the neutralino mass happens to lie near near a pole, such as $m_\chi \simeq m_Z/2$ or $m_h/2$, in which case there are large contributions to the annihilation through direct s-channel resonance exchange, the dominant contribution to the $\tilde{B}\tilde{B}$ annihilation cross section comes from crossed t-channel sfermion

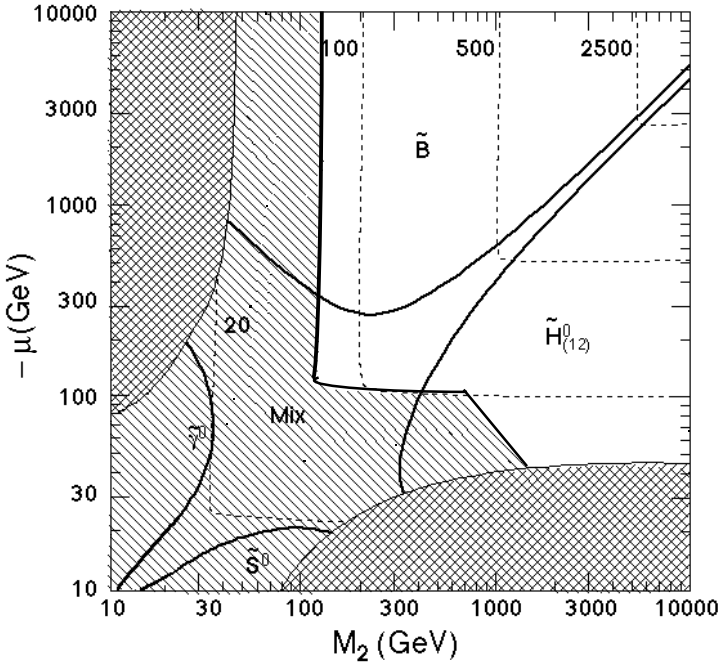

Figure 11. Mass contours and composition of nearly pure LSP states in the MSSM [117].

exchange.

Annihilations in the early Universe continue until the annihilation rate $\Gamma \simeq \sigma v n_\chi$ drops below the expansion rate. The calculation of the neutralino relic density proceeds in much the same way as discussed above for neutrinos with the appropriate substitution of the cross section. The final neutralino relic density expressed as a fraction of the critical energy density can be written as[111]

$$\Omega_\chi h^2 \simeq 1.9 \times 10^{-11} \left(\frac{T_\chi}{T_\gamma}\right)^3 N_f^{1/2} \left(\frac{\mathrm{GeV}}{a x_f + \frac{1}{2} b x_f^2}\right) \tag{53}$$

where $(T_\chi/T_\gamma)^3$ accounts for the subsequent reheating of the photon temperature with respect to χ, due to the annihilations of particles with mass $m < x_f m_\chi$ [100]. The subscript f refers to values at freeze-out, i.e., when annihilations cease. The coefficients a and b are related to the partial wave expansion of the cross-section, $\sigma v = a + bx + \ldots$. Eq. (53) results in a very good approximation to the relic density expect near s-channel annihilation

poles, thresholds and in regions where the LSP is nearly degenerate with the next lightest supersymmetric particle[120].

When there are several particle species i, which are nearly degenerate in mass, co-annihilations are important. In this case[120], the rate equation (41) still applies, provided n is interpreted as the total number density,

$$n \equiv \sum_i n_i \ , \tag{54}$$

n_0 as the total equilibrium number density,

$$n_0 \equiv \sum_i n_{0,i} \ , \tag{55}$$

and the effective annihilation cross section as

$$\langle \sigma_{\rm eff} v_{\rm rel} \rangle \equiv \sum_{ij} \frac{n_{0,i} n_{0,j}}{n_0^2} \langle \sigma_{ij} v_{\rm rel} \rangle \ . \tag{56}$$

In eq. (42), m_χ is now understood to be the mass of the lightest sparticle under consideration.

Note that this implies that the ratio of relic densities computed with and without coannihilations is, roughly,

$$R \equiv \frac{\Omega^0}{\Omega} \approx \left(\frac{\hat{\sigma}_{\rm eff}}{\hat{\sigma}_0} \right) \left(\frac{x_f}{x_f^0} \right) , \tag{57}$$

where $\hat{\sigma} \equiv a + bx/2$ and sub- and superscripts 0 denote quantities computed ignoring coannihilations. The ratio $x_f^0/x_f \approx 1 + x_f^0 \ln(g_{\rm eff}\sigma_{\rm eff}/g_1\sigma_0)$, where $g_{\rm eff} \equiv \sum_i g_i (m_i/m_1)^{3/2} e^{-(m_i - m_1)/T}$. For the case of three degenerate slepton NLSPs [121], $g_{\rm eff} = \sum_i g_i = 8$ and $x_f^0/x_f \approx 1.2$. The effects of co-annihilations are discussed below.

3.4. *Phenomenological and Cosmological Constraints*

For the cosmological limits on the relic density I will assume

$$0.1 \ \leq \ \Omega_\chi h^2 \ \leq \ 0.3. \tag{58}$$

The upper limit being a conservative bound based only on the lower limit to the age of the Universe of 12 Gyr. Indeed, most analyses indicate that $\Omega_{\rm matter} \lesssim 0.4 - 0.5$ and thus it is very likely that $\Omega_\chi h^2 < 0.2$ (cf. the CMB results in Table 1). One should note that smaller values of $\Omega_\chi h^2$ are allowed, since it is quite possible that some of the cold dark matter might not consist of LSPs.

The calculated relic density is found to have a relevant cosmological density over a wide range of susy parameters. For all values of $\tan\beta$, there is a 'bulk' region with relatively low values of $m_{1/2}$ and m_0 where $0.1 < \Omega_\chi h^2 < 0.3$. However there are a number of regions at large values of $m_{1/2}$ and/or m_0 where the relic density is still compatible with the cosmological constraints. At large values of $m_{1/2}$, the lighter stau, becomes nearly degenerate with the neutralino and co-annihilations between these particles must be taken into account[121,122]. For non-zero values of A_0, there are new regions for which $\chi - \tilde{t}$ coannihilations are important[123]. At large $\tan\beta$, as one increases $m_{1/2}$, the pseudo-scalar mass, m_A begins to drop so that there is a wide funnel-like region (at all values of m_0) such that $2m_\chi \approx m_A$ and s-channel annihilations become important[124,125]. Finally, there is a region at very high m_0 where the value of μ begins to fall and the LSP becomes more Higgsino-like. This is known as the 'focus point' region[126].

As an aid to the assessment of the prospects for detecting sparticles at different accelerators, benchmark sets of supersymmetric parameters have often been found useful, since they provide a focus for concentrated discussion. A set of proposed post-LEP benchmark scenarios[127] in the CMSSM are illustrated schematically in Fig. 12. Five of the chosen points are in the 'bulk' region at small $m_{1/2}$ and m_0, four are spread along the coannihilation 'tail' at larger $m_{1/2}$ for various values of $\tan\beta$. This tail runs along the shaded region in the lower right corner where the stau is the LSP and is therefore excluded by the constraints against charged dark matter. Two points are in rapid-annihilation 'funnels' at large $m_{1/2}$ and m_0. At large values of m_0, the focus-point region runs along the boundary where electroweak symmetry no longer occurs (shown in Fig. 12 as the shaded region in the upper left corner). Two points were chosen in the focus-point region at large m_0. The proposed points range over the allowed values of $\tan\beta$ between 5 and 50. The light shaded region corresponds to the portion of parameter space where the relic density $\Omega_\chi h^2$ is between 0.1 and 0.3.

The effect of coannihilations is to create an allowed band about 25-50 GeV wide in m_0 for $m_{1/2} \lesssim 1400$ GeV, which tracks above the $m_{\tilde{\tau}} = m_\chi$ contour. Along the line $m_{\tilde{\tau}} = m_\chi$, $R \approx 10$, from (57) [121]. As m_0 increases, the mass difference increases and the slepton contribution to $\hat{\sigma}_{\rm eff}$ falls, and the relic density rises abruptly. This effect is seen in Fig. 13. The light shaded region corresponds to $0.1 < \Omega h^2 < 0.3$. The dark shaded region has $m_{\tilde{\tau}} < m_\chi$ and is excluded. The light dashed contours indicate the corresponding region in Ωh^2 if one ignores the effect of coannihilations.

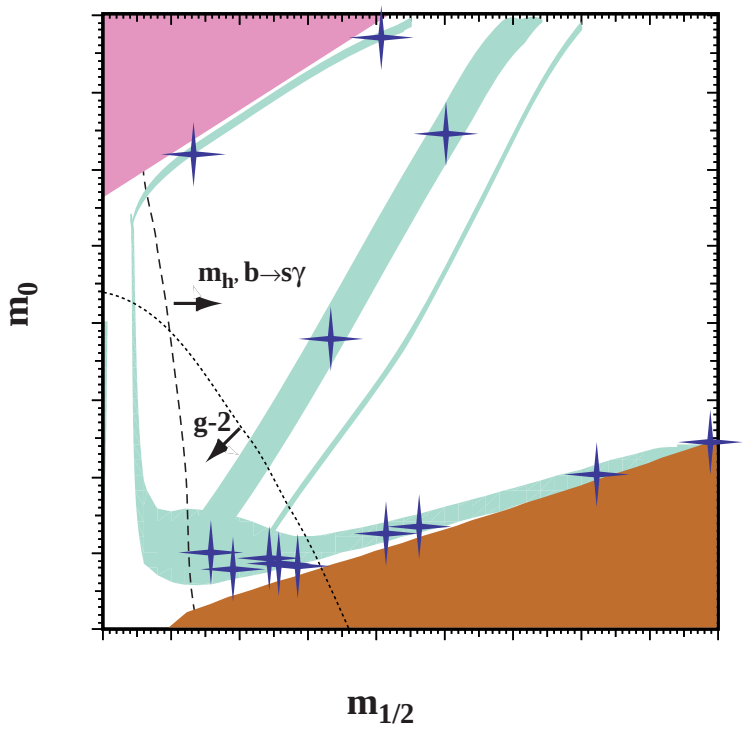

Figure 12. Schematic overview of the CMSSM benchmark points proposed in [127]. The points are intended to illustrate the range of available possibilities. The labels correspond to the approximate positions of the benchmark points in the $(m_{1/2}, m_0)$ plane. They also span values of $\tan\beta$ from 5 to 50 and include points with $\mu < 0$.

Neglecting coannihilations, one would find an upper bound of ~ 450 GeV on $m_{1/2}$, corresponding to an upper bound of roughly 200 GeV on $m_{\tilde{B}}$. Instead, values of $m_{1/2}$ up to ~ 1400 GeV are allowed corresponding to an upper bound of ~ 600 GeV on $m_{\tilde{B}}$.

The most important phenomenological constraints are also shown schematically in Figure 12. These include the constraint provided by the LEP lower limit on the Higgs mass: $m_H > 114.4$ GeV [128]. This holds in the Standard Model, for the lightest Higgs boson h in the general MSSM for $\tan\beta \lesssim 8$, and almost always in the CMSSM for all $\tan\beta$. Since m_h is sensitive to sparticle masses, particularly $m_{\tilde{t}}$, via loop corrections, the Higgs limit also imposes important constraints on the CMSSM parameters, principally $m_{1/2}$ as seen by the dashed curve in Fig. 12.

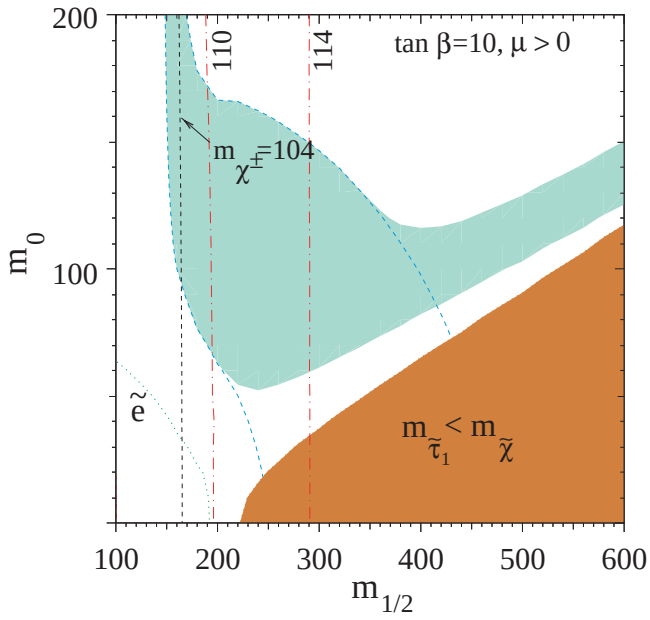

Figure 13. The light-shaded 'bulk' area is the cosmologically preferred region with $0.1 \leq \Omega h^2 \leq 0.3$. The light dashed lines show the location of the cosmologically preferred region if one ignores coannihilations with the light sleptons. In the dark shaded region in the bottom right, the LSP is the $\tilde{\tau}_1$, leading to an unacceptable abundance of charged dark matter. Also shown is the isomass contour $m_{\chi^\pm} = 104$ GeV and $m_h = 110, 114$ GeV, as well as an indication of the slepton bound from LEP.

The constraint imposed by measurements of $b \to s\gamma$ [129] also exclude small values of $m_{1/2}$. These measurements agree with the Standard Model, and therefore provide bounds on MSSM particles, such as the chargino and charged Higgs masses, in particular. Typically, the $b \to s\gamma$ constraint is more important for $\mu < 0$, but it is also relevant for $\mu > 0$, particularly when $\tan\beta$ is large. The BNL E821 experiment reported last year a new measurement of $a_\mu \equiv \frac{1}{2}(g_\mu - 2)$ which deviated by 2.6 standard deviations from the best Standard Model prediction available at that time[130]. However, it had been realized that the sign of the most important pseudoscalar-meson pole part of the light-by-light scattering contribution[131] to the Standard Model prediction should be reversed, which reduces the apparent experimental discrepancy to about 1.6 standard deviations ($\delta a_\mu \times 10^{10} = 26 \pm 16$). The largest contribution to the errors in the comparison with theory was

thought to be the statistical error of the experiment, which has been significantly reduced just recently[132]. The world average of $a_\mu \equiv \frac{1}{2}(g_\mu - 2)$ now deviates by $(33.9 \pm 11.2) \times 10^{-10}$ from the Standard Model calculation of Davier et al.[133] using e^+e^- data, and by $(17 \pm 11) \times 10^{-10}$ from the Standard Model calculation of Davier et al.[133] based on τ decay data. Other recent analyses of the e^+e^- data yield similar results. On the subsequent plots, the formal 2-σ range $11.5 \times 10^{-10} < \delta a_\mu < 56.3 \times 10^{-10}$ is displayed.

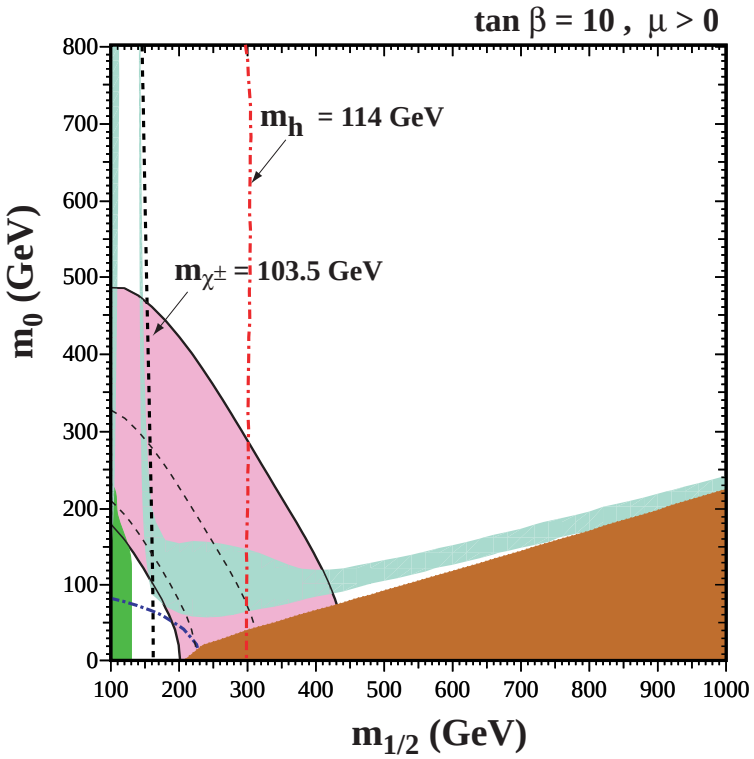

Figure 14. Compilation of phenomenological constraints on the CMSSM for $\tan\beta = 10, \mu > 0$, assuming $A_0 = 0, m_t = 175$ GeV and $m_b(m_b)^{\overline{MS}}_{SM} = 4.25$ GeV. The near-vertical lines are the LEP limits $m_{\chi^\pm} = 103.5$ GeV (dashed and black)[119], and $m_h = 114.1$ GeV (dotted and red)[128]. Also, in the lower left corner we show the $m_{\tilde{e}} = 99$ GeV contour[135]. In the dark (brick red) shaded regions, the LSP is the charged $\tilde{\tau}_1$, so this region is excluded. The light(turquoise) shaded areas are the cosmologically preferred regions with $0.1 \leq \Omega h^2 \leq 0.3$ [125]. The medium (dark green) shaded regions are excluded by $b \to s\gamma$ [129]. The shaded (pink) region in the upper right delineates the $2\,\sigma$ range of $g_\mu - 2$. The dashed curves within this region correspond to the $1 - \sigma$ bounds.

Following a previous analysis[125,134], in Figure 14 the $m_{1/2} - m_0$ parameter space is shown for $\tan\beta = 10$. The dark shaded region (in the lower right) corresponds to the parameters where the LSP is not a neutralino but rather a $\tilde{\tau}_R$. The cosmologically interesting region at the left of the figure is due to the appearance of pole effects. There, the LSP can annihilate through s-channel Z and h (the light Higgs) exchange, thereby allowing a very large value of m_0. However, this region is excluded by phenomenological constraints. Here one can see clearly the coannihilation tail which extends towards large values of $m_{1/2}$. In addition to the phenomenological constraints discussed above, Figure 14 also shows the current experimental constraints on the CMSSM parameter space due to the limit $m_{\chi^\pm} \gtrsim 103.5$ GeV provided by chargino searches at LEP [119]. LEP has also provided lower limits on slepton masses, of which the strongest is $m_{\tilde{e}} \gtrsim 99$ GeV [135]. This is shown by dot-dashed curve in the lower left corner of Fig. 14. Similar results have been found by other analyses[136].

As one can see, one of the most important phenomenological constraint at this value of $\tan\beta$ is due to the Higgs mass (shown by the nearly vertical dot-dashed curve). The theoretical Higgs masses were evaluated using `FeynHiggs`[137], which is estimated to have a residual uncertainty of a couple of GeV in m_h. The region excluded by the $b \to s\gamma$ constraint is the dark shaded (green) region to the left of the plot. As many authors have pointed out[138], a discrepancy between theory and the BNL experiment could well be explained by supersymmetry. As seen in Fig. 14, this is particularly easy if $\mu > 0$. The medium (pink) shaded region in the figure corresponds to the overall allowed region (2σ) by the new experimental result.

As discussed above, another mechanism for extending the allowed CMSSM region to large m_χ is rapid annihilation via a direct-channel pole when $m_\chi \sim \frac{1}{2} m_A$ [124,125]. This may yield a 'funnel' extending to large $m_{1/2}$ and m_0 at large $\tan\beta$, as seen in Fig. 15.

In principle, the true input parameters in the CMSSM are: μ, m_1, m_2, and B, where m_1 and m_2 are the Higgs soft masses (in the CMSSM $m_1 = m_2 = m_0$ and B is the susy breaking bilinear mass term). In this case, the electroweak symmetry breaking conditions lead to a prediction of $M_Z, \tan\beta$,and m_A. Since we are not really interested in predicting M_Z, it is more useful to assume instead the following CMSSM input parameters: M_Z, m_1, m_2, and $\tan\beta$ again with $m_1 = m_2 = m_0$. In this case, one predicts μ, B, and m_A. However, one can generalize the CMSSM case to include non-universal Higgs masses[139,140] (NUHM), in which case the input parameters become:M_Z, μ, m_A, and $\tan\beta$ and one predicts m_1, m_2, and B.

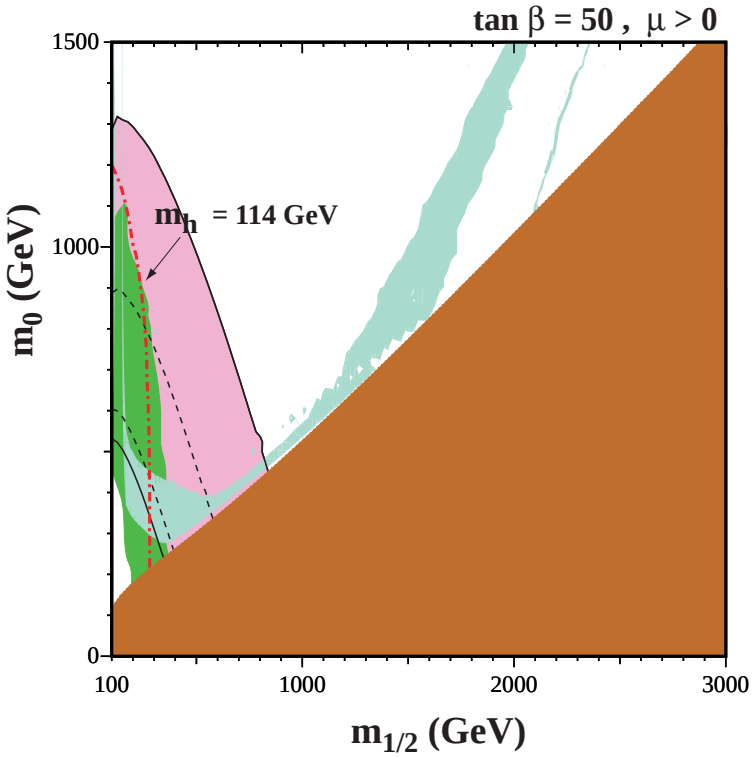

Figure 15. As in Fig. 14 for $\tan\beta = 50$.

The NUHM parameter space was recently analyzed[140] and a sample of the results found is shown in Fig. 16. While much of the cosmologically preferred area with $\mu < 0$ is excluded, there is a significant enhancement in the allowed parameter space for $\mu > 0$.

3.5. *Detection*

Because the LSP as dark matter is present locally, there are many avenues for pursuing dark matter detection. Direct detection techniques rely on an ample neutralino-nucleon scattering cross-section. The effective four-fermion lagrangian can be written as

$$\mathcal{L} = \bar{\chi}\gamma^{\mu}\gamma^{5}\chi\bar{q}_i\gamma_{\mu}(\alpha_{1i} + \alpha_{2i}\gamma^{5})q_i + \alpha_{3i}\bar{\chi}\chi\bar{q}_i q_i + \alpha_{4i}\bar{\chi}\gamma^{5}\chi\bar{q}_i\gamma^{5}q_i$$

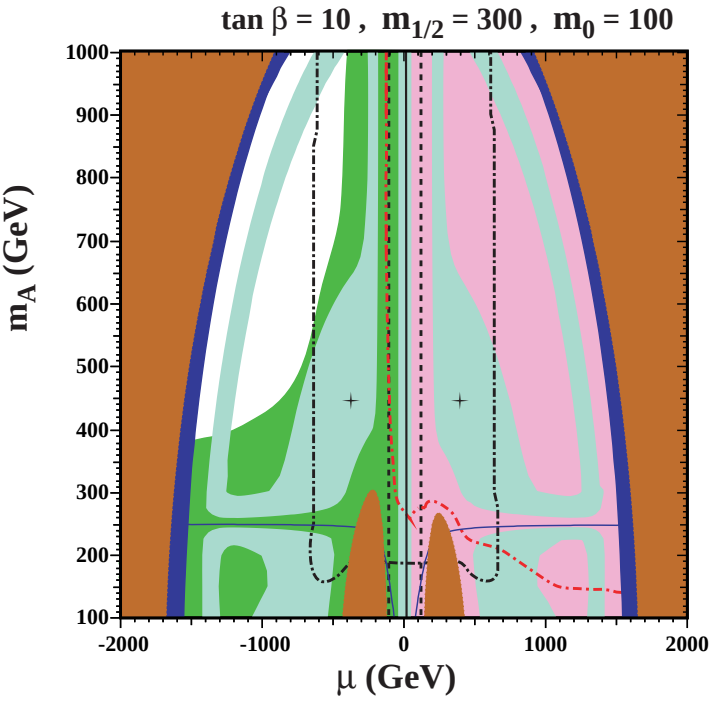

Figure 16. Compilations of phenomenological constraints on the MSSM with NUHM in the (μ, m_A) plane for $\tan\beta = 10$ and $m_0 = 100$ GeV, $m_{1/2} = 300$ GeV, assuming $A_0 = 0$, $m_t = 175$ GeV and $m_b(m_b)^{\overline{MS}}_{SM} = 4.25$ GeV. The shading is as described in Fig. 14. The (blue) solid line is the contour $m_\chi = m_A/2$, near which rapid direct-channel annihilation suppresses the relic density. The dark (black) dot-dashed line indicates when one or another Higgs mass-squared becomes negative at the GUT scale: only lower $|\mu|$ and larger m_A values are allowed. The crosses denote the values of μ and m_A found in the CMSSM.

$$+ \alpha_{5i}\bar{\chi}\chi\bar{q}_i\gamma^5 q_i + \alpha_{6i}\bar{\chi}\gamma^5\chi\bar{q}_i q_i \tag{59}$$

However, the terms involving $\alpha_{1i}, \alpha_{4i}, \alpha_{5i}$, and α_{6i} lead to velocity dependent elastic cross sections. The remaining terms are: the spin dependent coefficient, α_{2i} and the scalar coefficient α_{3i}. Contributions to α_{2i} are predominantly through light squark exchange. This is the dominant channel for binos. Scattering also occurs through Z exchange but this channel requires a strong Higgsino component. Contributions to α_{3i} are also dominated by light squark exchange but Higgs exchange is non-negligible in most cases.

Fig. 17 displays contours of the spin-independent cross section for the

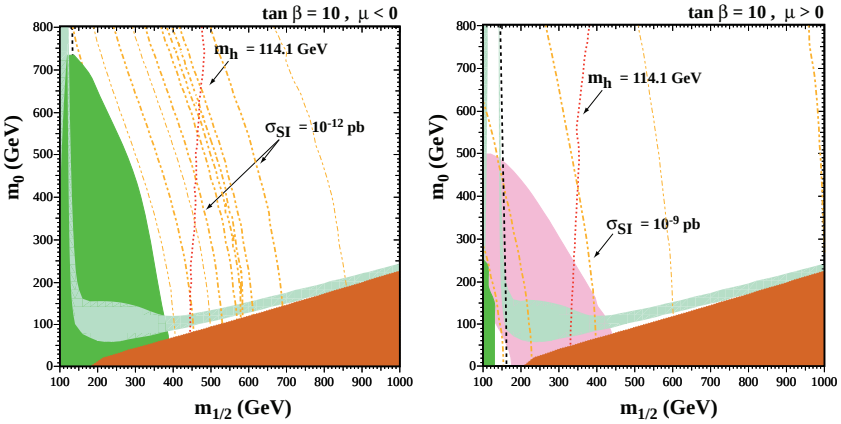

Figure 17. *Spin-independent cross sections in the* $(m_{1/2}, m_0)$ *planes for (a)* $\tan\beta = 10, \mu < 0$*, (b)* $\tan\beta = 10, \mu > 0$*. The double dot-dashed (orange) curves are contours of the spin-independent cross section, differing by factors of 10 (bolder) and interpolating factors of 3 (finer - when shown). For example, in (b), the curves to the right of the one marked* 10^{-9} *pb correspond to* 3×10^{-10} *pb and* 10^{-10} *pb.*

elastic scattering of the LSP χ on protons in the $m_{1/2}, m_0$ planes for (a) $\tan\beta = 10, \mu < 0$, (b) $\tan\beta = 10, \mu > 0$ [141]. The double dot-dashed (orange) lines are contours of the spin-independent cross section, and the contours $\sigma_{SI} = 10^{-9}$ pb in panel (a) and $\sigma_{SI} = 10^{-12}$ pb in panel (b) are indicated. The LEP lower limits on m_h and $m_{\chi^\pm}$, as well as the experimental measurement of $b \to s\gamma$ for $\mu < 0$, tend to bound the cross sections from above, as discussed in more detail below. Generally speaking, the spin-independent cross section is relatively large in the 'bulk' region, but falls off in the coannihilation 'tail'. Also, we note also that there is a strong cancellation in the spin-independent cross section when $\mu < 0$ [142,143], as seen along strips in panel (a) of Fig. 17 where $m_{1/2} \sim 500$ GeV. In the cancellation region, the cross section drops lower than 10^{-14} pb. All these possibilities for suppressed spin-independent cross sections are disfavoured by the data on $g_\mu - 2$, which favour values of $m_{1/2}$ and m_0 that are not very large, as well as $\mu > 0$, as seen in panel (b) of Fig. 17. Thus $g_\mu - 2$ tends to provide a lower bound on the spin-independent cross section.

Fig. 18(a) illustrates the effect on the cross sections of each of the principal phenomenological constraints, for the particular case $\tan\beta = 10$ $\mu > 0$. The solid (blue) lines mark the bounds on the cross sections allowed by the relic-density constraint $0.1 < \Omega_\chi h^2 < 0.3$ alone. For any given value of

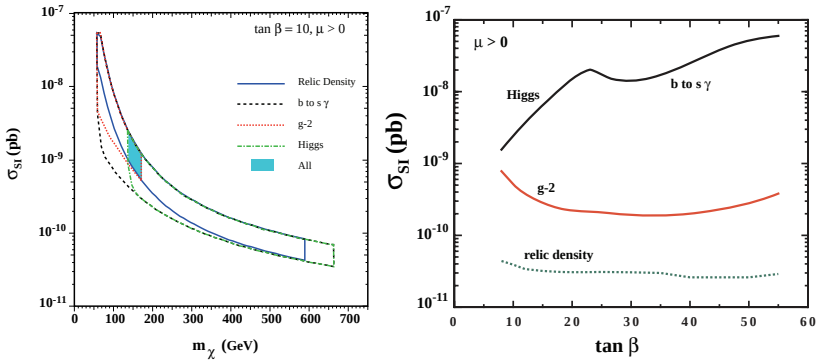

Figure 18. *Allowed ranges of the cross sections for* $\tan\beta = 10$ *(a)* $\mu > 0$ *for spin-independent elastic scattering. The solid (blue) lines indicate the relic density constraint, the dashed (black) lines the* $b \to s\gamma$ *constraint, the dot-dashed (green) lines the* m_h *constraint, and the dotted (red) lines the* $g_\mu - 2$ *constraint. The shaded (pale blue) region is allowed by all the constraints. (b) The allowed ranges of the spin-independent cross section for* $\mu > 0$*. The darker solid (black) lines show the upper limits on the cross sections obtained from* m_h *and* $b \to s\gamma$*, and (where applicable) the lighter solid (red) lines show the lower limits suggested by* $g_\mu - 2$ *and the dotted (green) lines the lower limits from the relic density.*

$m_{1/2}$, only a restricted range of m_0 is allowed. Therefore, only a limited range of m_0, and hence only a limited range for the cross section, is allowed for any given value of m_χ. The thicknesses of the allowed regions are due in part to the assumed uncertainties in the nuclear inputs. These have been discussed at length in [143,142]. On the other hand, a broad range of m_χ is allowed, when one takes into account the coannihilation 'tail' region at each $\tan\beta$ and the rapid-annihilation 'funnel' regions for $\tan\beta = 35, 50$. The dashed (black) line displays the range allowed by the $b \to s\gamma$ constraint alone. In this case, a broader range of m_0 and hence the spin-independent cross section is possible for any given value of m_χ. The impact of the constraint due to m_h is shown by the dot-dashed (green) line. Comparing with the previous constraints, we see that a region at low m_χ is excluded by m_h, strengthening significantly the previous *upper* limit on the spin-independent cross section. Finally, the dotted (red) lines in Fig. 18 show the impact of the $g_\mu - 2$ constraint. This imposes an upper bound on $m_{1/2}$ and hence m_χ, and correspondingly a *lower* limit on the spin-independent cross section.

This analysis is extended in panel (b) of Fig. 18 to all the values $8 < \tan\beta \leq 55$ and we find overall that [141]

$$2 \times 10^{-10}\ \text{pb} \lesssim \sigma_{SI} \lesssim 6 \times 10^{-8}\ \text{pb}, \tag{60}$$

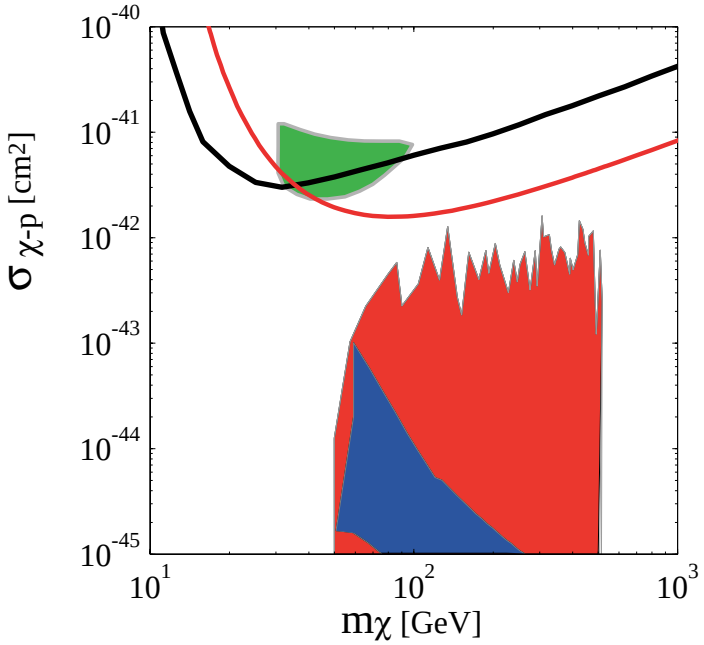

Figure 19. Limits from the CDMS[145] and Edelweiss[146] experiments on the neutralino-proton elastic scattering cross section as a function of the neutralino mass. The Edelweiss limit is stronger at higher m_χ. These results nearly exclude the shaded region observed by DAMA[147]. The theoretical predictions lie at lower values of the cross section.

$$2 \times 10^{-7} \text{ pb} \lesssim \sigma_{SD} \lesssim 10^{-5} \text{ pb}, \tag{61}$$

for $\mu > 0$. (σ_{SD} is the spin-dependent cross-section not shown in the figures presented here.) As we see in panel (b) of Fig. 18, m_h provides the most important upper limit on the cross sections for $\tan\beta < 23$, and $b \to s\gamma$ for larger $\tan\beta$, with $g_\mu - 2$ always providing a more stringent lower limit than the relic-density constraint. The relic density constraint shown is evaluated at the endpoint of the coannihilation region. At large $\tan\beta$, the Higgs funnels or the focus-point regions have not been considered, as their locations are very sensitive to input parameters and calculational details[144].

The results from a CMSSM and MSSM analysis[142,143] for $\tan\beta = 3$ and 10 are compared with the most recent CDMS[145] and Edelweiss[146] bounds in Fig. 19. These results have nearly entirely excluded the region purported by the DAMA[147] experiment. The CMSSM prediction[142] is shown by the dark shaded region, while the NUHM case[143] is shown by the larger lighter

shaded region. Other CMSSM results[148] are also available.

I conclude by showing the prospects for direct detection for the benchmark points discussed above[149]. Fig. 20 shows rates for the elastic spin-independent scattering of supersymmetric relics, including the projected sensitivities for CDMS II[150] and CRESST[151] (solid) and GENIUS[152] (dashed). Also shown are the cross sections calculated in the proposed benchmark scenarios discussed in the previous section, which are considerably below the DAMA[147] range ($10^{-5} - 10^{-6}$ pb). Indirect searches for supersymmetric dark matter via the products of annihilations in the galactic halo or inside the Sun also have prospects in some of the benchmark scenarios[149].

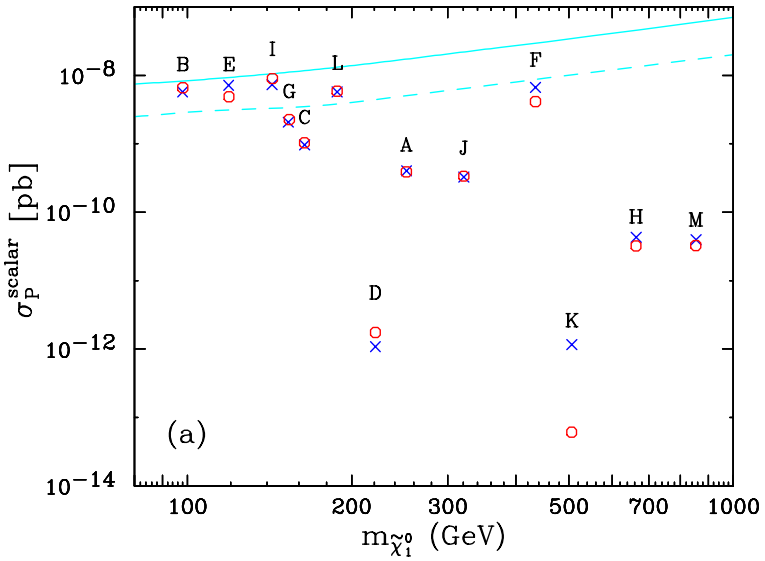

Figure 20. Elastic spin-independent scattering of supersymmetric relics on protons calculated in benchmark scenarios[149], compared with the projected sensitivities for CDMS II [150] and CRESST[151] (solid) and GENIUS[152] (dashed). The predictions of our code (blue crosses) and `Neutdriver`[153] (red circles) for neutralino-nucleon scattering are compared. The labels A, B, ...,L correspond to the benchmark points as shown in Fig. 12.

References

1. F. Zwicky, *Helv. Phys. Acta.* **6** (1933) 110.
2. S. Folkes *et al.*, *MNRAS* **308** (1999) 459; M. L. Blanton *et al.*, *Astr. J.* **121** (2001) 2358.

3. S. M. Faber and J. J. Gallagher, *Ann. Rev. Astron. Astrophys.* **17** (1979) 135.
4. A. Bosma, *Ap. J.* **86** (1981) 1825; V. C. Rubin, W. K. Ford and N. Thonnard, *Ap. J.* **238** (1980) 471; V. C. Rubin, D. Burstein, W. K. Ford and N. Thonnard, *Ap. J.* **289** (1985) 81; T. S. Van Albada and R. Sancisi, *Phil. Trans. R. Soc. Land.* **A320** (1986) 447.
5. M. Persic and P. Salucci, *Ap. J. Supp.* **99** (1995) 501; M. Persic, P. Salucci, and F. Stel, *MNRAS* **281** (1996) 27P.
6. R. P. Saglia *et al.*, *Ap. J.* **403** (1993) 567; C. M. Carollo *et al.*, *Ap. J.* **411** (1995) 25; A. Borriello, P. Salucci, and L. Danese, astro-ph/0208268.
7. D. Fabricant and P. Gorenstein, *Ap. J.* **267** (1983) 535; G. C. Stewart, C. R. Canizares, A. C. Fabian and P. E. J. Nilsen, *Ap. J.* **278** (1984) 53 and references therein.
8. W. Forman, C. Jones, and W. Tucker, *Ap. J.* **293** (1985) 102; A. C. Fabian, P. A. Thomas, S. M. Fall, and R. E. White III, *MNRAS* **221** (1986) 1049; M. Loewenstein and R. E. White, *Ap. J.* **518** (1999) 50; M. Loewenstein and R. F. Mushotzky, astro-ph/0208090.
9. R. Mushotzky, in *Relativistic Astrophysics and Particle Cosmology* ed. C. W. Akerlof and M. Srednicki (New York Academy of Sciences, New York, 1993), p. 184; J. S. Mulchaey, D. S. Davis, R. F. Mushotzky, and D. Burstein, *Ap. J.* **404** (1993) L9; M. J. Henriksen and G. A. Mamon, *Ap. J.* **421** (1994) L63; L. P. David, C. Jones, and W. Foreman, *Ap. J.* **445** (1995) 578.
10. S. D. M. White, J. F. Navarro, A. E. Evrard, and C. S. Frenk, *Nature* **366** (1993) 429; S. Schindler, *A. A.* **305** (1996) 756.
11. J. A. Tyson, F. Valdes, and R. A. Wenk, *Ap. J.* **349** (1990) L1.
12. E. Turner, J. Ostriker, and J. Gott III, *Ap. J.* **284** (1984) 1.
13. G. Golse, J.-P. Kneib, and G. Soucail, *A. A.* **387** (2002) 788.
14. R. Blanford and R. Narayan, *Ann. Rev. A. A.* **30** (1992) 311.
15. P. Fischer *et al.*, *Astr. J.* **120** (2000) 1198; D. Smith, G. Bernstein, P. Fischer, and M. Jarvis, *Ap. J.* **551** (2001) 641; N. Straumann, *Sp. Sci. Rev.* **100** (2002) 29.
16. Y. Mellier, *Ann. Rev. Ast. Astr.* **37** (1999) 127.
17. L. van Waerbeke, Y. Mellier, and M. Radovich, *A. A.* **374** (2001) 757.
18. T. Erben *et al.*, *A. A.* **355** (2000) 23; K. Umetsu and T. Futamase, *Ap. J.* **539** (2000) 5; H. Bonnet, Y. Mellier, and B. Fort, *Ap. J.* **427** (1994) L83.
19. Y. Mellier, *Sp. Sci. Rev.* **100** (2002) 73.
20. P. J. E. Peebles, *The Large Scale Structure of the Universe*, (Princeton University Press, Princeton, 1980).
21. A. Dressler, D. Lynden-Bell D. Burstein, R. Davies, S. Faber, R. Terlevich, and G. Wegner, *Ap. J.* **313** (1987) L37; A. Dekel, E. Bertschinger, A. Yahil, M. A. Strauss, M. Davis, and J. P. Huchra, *Ap. J.* **412** (1993) 1.
22. J. A Willick, M. A. Strauss, A. Dekel, and T. Kolatt, *Ap. J.* **486** (1997) 629; J. A Willick and M. A. Strauss *A. A.* **507** (1998) 64.
23. Y. Sigad, A. Eldar, A. Dekel, M. A. Strauss, and A. Yahill, *Ap. J.* **495** (1998) 516; E. Branchini, I. Zehavi, M. Plionis, and A. Dekel, *MNRAS* **313** (2000) 491.
24. S. Schindler, *Sp. Sci. Rev.* **100** (2002) 299.

25. R. A. Alpher and R. C. Herman, *Phys. Rev.* **74**, 1737 (1948); *Phys. Rev.* **75**, 1089 (1949).
26. A. T. Lee *et al.*, *Ap. J.* **561** (2001) L1 [arXiv:astro-ph/0104459].
27. C. B. Netterfield *et al.* [Boomerang Collaboration], *Ap. J.* **571** (2002) 604 [arXiv:astro-ph/0104460].
28. N. W. Halverson *et al. MNRAS* **568** (2002) 38 [arXiv:astro-ph/0104489].
29. R. Stompor *et al.*, *Ap.J.* **561** (2001) L7 [arXiv:astro-ph/0105062].
30. C. Pryke, N. W. Halverson, E. M. Leitch, J. Kovac, J. E. Carlstrom, W. L. Holzapfel and M. Dragovan, *Ap. J.* **568** (2002) 46 [arXiv:astro-ph/0104490].
31. S. Padin, *et al. Ap.J.* **549** (2001) L1.
32. J. A. Rubino-Martin *et al.*, arXiv:astro-ph/0205367.
33. A. Benoit *et al.* [Archeops Collaboration], arXiv:astro-ph/0210306.
34. M. E. Abroe *et al.*, *MNRAS* **334** (2002) 11 [arXiv:astro-ph/0111010].
35. W. L. Freedman *et al.*, *Ap.J.* **553** (2001) 47.
36. A. G. Riess *et al.*, *A. J.* **116** (1998) 1009; S. Perlmutter *et al.*, *Ap. J.* **517** (1999) 565; A. G. Riess, *PASP* **112** (2000) 1284.
37. K. A. Olive and J. A. Peacock, *Phys. Rev.* **D66** (2002) 010001.
38. for reviews see: A. D. Linde, *Particle Physics And Inflationary Cosmology* Harwood (1990); K. A. Olive, *Phys. Rep.* **190** (1990) 307; D. H. Lyth and A. Riotto, *Phys. Rept.* **314** (1999) 1 [arXiv:hep-ph/9807278].
39. W.H. Press, *Phys. Scr.* **21** (1980) 702; V. F. Mukhanov and G. V. Chibisov, *JETP Lett.* **33** (1981) 532; S. W. Hawking, *Phys. Lett.* **115B** (1982) 295; A. A. Starobinsky, , *Phys. Lett.* **117B** (1982) 175; A. H. Guth and S.Y. Pi, *Phys. Rev. Lett.* **49** (1982) 1110; J. M. Bardeen, P. J. Steinhardt and M. S. Turner, *Phys. Rev.* **D28** (1983) 679.
40. E. R. Harrison, *Phys. Rev.* **D1** (1979) 2726; Ya. B. Zeldovich, *MNRAS* **160** (1972) 1P.
41. E. L. Wright *et al. Ap.J.* **396** (1992) L13; G. Hinshaw *et al.*, *Ap. J.* **464** (1996) L17; G. F. Smoot and D. Scott, *Phys. Rev.* **D66** (2002) 010001.
42. J. R. Bond and A. S. Szalay, *Ap.J.* **274** (1983) 443.
43. J. R. Bond, G. Efstathiou and J. Silk, *Phys. Lett.* **45** (1980) 1980; Ya. B. Zeldovich and R. A.Sunyaev, *Sov. Ast. Lett.* **6** (1980) 457.
44. T. P. Walker, G. Steigman, D. N. Schramm, K. A. Olive and K. Kang, *Ap.J.* **376** (1991) 51; S. Sarkar, *Rep. Prog. Phys.* **59** (1996) 1493; K. A. Olive, G. Steigman, and T. P. Walker, *Phys. Rep.* **333** (2000) 389; B. D. Fields and S. Sarkar, *Phys. Rev.* **D66** (2002) 010001.
45. L. M. Krauss and P. Romanelli, *Ap.J.* **358** (1990) 47; M. Smith, L. Kawano, and R. A. Malaney, *Ap.J. Supp.* **85** (1993) 219; N. Hata, R. J. Scherrer, G. Steigman, D. Thomas, and T. P. Walker, *Ap.J.* **458** (1996) 637; A. Coc, E. Vangioni-Flam, M. Casse and M. Rabiet, *Phys. Rev.* **D65** (2002) 043510; K. M. Nollett and S. Burles, *Phys. Rev.* **D61** (2000) 123505 [arXiv:astro-ph/0001440].
46. R. H. Cyburt, B. D. Fields, and K. A. Olive, *New Ast.* **6** (1996) 215 [arXiv:astro-ph/0102179].
47. B. D. Fields and K. A. Olive, *Ap. J.* **506** (1998) 177 [arXiv:astro-ph/9803297].

48. K.A. Olive, and E. Skillman, *New Ast.* **6** (2001) 119 [arXiv:astro-ph/0007081].
49. Y. I. Izotov and T. X. Thuan, *Ap. J.* **500** (1998) 188; Y. I. Izotov, T. X. Thuan, and V. A. Lipovetsky, *Ap. J.* **108** (1997) 1; Y. I. Izotov, T. X. Thuan, and V. A. Lipovetsky, *Ap. J.* **435** (1994) 647.
50. M. Peimbert, A. Peimbert and M. T. Ruiz, *Ap. J.* **541** (2000) 688; A. Peimbert, M. Peimbert and V. Luridiana, *Ap. J.* **565** (2002) 668.
51. S. G. Ryan *et al.*, *Ap. J.* **523** (2000) L57.
52. P. Bonifacio, *et al.*, *A. A.* **390** (2002) 91.
53. J. M. O'Meara, D. Tytler, D. Kirkman, N. Suzuki, J. X. Prochaska, D. Lubin and A. M. Wolfe, *Ap. J.* **552** (2001) 718 [arXiv:astro-ph/0011179].
54. D. Tytler, J. M. O'Meara, N. Suzuki, and D. Lubin, *Phys. Rep.* **333** (2000) 409.
55. M. Pettini and D. V. Bowen, *Ap. J.* **560** (2001) 41 [arXiv:astro-ph/0104474]; S. D'Odorico, M. Dessauges-Zavadsky, and P. Molaro, *A. A.* **368** (2001) L21.
56. B. D. Fields, K. A. Olive, J. Silk, M. Cassé and E. Vangioni-Flam, *Ap. J.* **563** (2001) 653 [arXiv:astro-ph/0107389].
57. H. Reeves, J. Audouze, W. Fowler, and D. N. Schramm, *Ap. J.* **179** (1976) 909.
58. T. M. Bania, R. T. Rood and D. S. Balser, *Nature* **415** (2002) 54.
59. E. Vangioni-Flam, K. A. Olive, B. D. Fields and M. Casse, arXiv:astro-ph/0207583.
60. M. Persic and P. Salucci, *MNRAS* **258** (1992) 14p.
61. M. Fukugita, C. J. Hogan, and P. J. E. Peebles, *Ap. J.* **503** (1998) 518.
62. M. G. Haehnelt, P. Madau, R. Kudritzki, and F. Haardt, *Ap. J.* **549** (2001) L151; D. Reimers, *Sp. Sci. Rev.* **100** (2002) 89.
63. D. J. Hegyi and K. A. Olive, *Phys. Lett.* **126B** (1983) 28; *Ap. J.* **303** (1986) 56.
64. C. Low and D. Lynden-Bell, *MNRAS* **176** (1976) 367; M. J. Rees, *MNRAS* **176** (1976) 483; J. Silk, *Ap. J.* **256** (1982) 514; F. Palla, E. E. Salpeter and S. W. Stahler, *Ap. J.* **271** (1983) 632.
65. J.M. Scalo, *Fund. Comm. Phys.* **11** (1986) 1.
66. D. J. Hegyi and G. L. Gerber, *Ap. J.* **218** (1987) L7; D. J. Hegyi, in *Proc. of 1st Moriond Astrophysics Meeting*, Audouze, P. Crane, D. Hegyi, and J. Tran. Than Van, eds., (Dreux, France:Frontiers) 1981, p. 321; S. P. Boughn, P. R. Saulson, and M. Seldner,*Ap. J.* **250** (1981) L15.
67. B. Paczynski, *Ap. J.* **304** (1986) 1.
68. C. Alcock *et al.*, *Nature* **365** (1983) 621; E. Aubourg *et al. Nature* **365** (1983) 623.
69. C. Alcock *et al.*, *Ap. J* . **542** (2000) 281.
70. T. Lasserre, *et al.*, *A. A.* **355** (2000) 39L; C. Afonso *et al.*, astro-ph/0212176.
71. B. J. Carr, *Ann. Rev. Astron. Astrophys.* **32** (1994) 531; astro-ph/0102389.
72. D. S. Ryu, K. A. Olive and J. Silk, *Ap. J.* **353** (1990) 81.
73. B. D. Fields, K. Freese, and D. S. Graf, *Ap. J.* **534** (2000) 265.
74. J. H. MacGibbon, *Nature* **329** (1987) 308.
75. B. J. Carr, J. R. Bond and W. D. Arnett, *Ap. J.* **277** (1984) 445; J. R. Bond,

W. D. Arnett and B. J. Carr, *Ap. J.* **280** (1984) 825; W. W. Ober, M. F. El Eid and K. J. Fricke, *A. A.* **119** (1983) 61.
76. C. G. Lacey, and J. P. Ostriker, *Ap. J.* **299** (1985) 633.
77. H.-W. Rix and G. Lake, *Ap. J.* **417** (1993) L1.
78. D. N. Schramm and G. Steigman, *Ap. J.* **243** (1981) 1.
79. P. J. E. Peebles, *Ap. J.* **258** (1982) 415; A. Melott, *MNRAS* **202** (1983) 595; A. A. Klypin, S. F. Shandarin, *MNRAS* **204** (1983) 891.
80. C. S. Frenk, S. D. M. White and M.Davis, *Ap. J.* **271** (1983) 417.
81. S. D. M. White, C. S. Frenk and M. Davis, *Ap. J.* **274** (1983) 61.
82. J. R. Bond, J. Centrella, A. S. Szalay and J. Wilson, in *Formation and Evolution of Galaxies and Large Structures in the Universe*, ed. J. Andouze and J. Tran Thanh Van, (Dordrecht-Reidel 1983) p. 87.
83. K. Enqvist, K. Kainulainen and V. Semikoz, *Nucl. Phys.* **B374** (1992) 392.
84. S. S. Gerstein and Ya. B. Zeldovich, *JETP Lett.* **4** (1966) 647; R. Cowsik and J. McClelland, *Phys. Rev. Lett.* **29** (1972) 669; A. S. Szalay and G. Marx, *A. A.* **49** (1976) 437.
85. K. Kainulainen and K. A. Olive, arXiv:hep-ph/0206163.
86. R. A. Croft, W. Hu and R. Dave, *Phys. Rev. Lett.* **83** (1999) 1092 [arXiv:astro-ph/9903335].
87. X. M. Wang, M. Tegmark and M. Zaldarriaga, *Phys. Rev.* **D65** (2002) 123001 [arXiv:astro-ph/0105091].
88. Ø. Elgaroy *et al.*, *Phys. Rev. Lett.* **89** (2002) 061301 [arXiv:astro-ph/0204152].
89. A. Lewis and S. Bridle, *Phys. Rev.* **D66** (2002) 103511 [arXiv:astro-ph/0205436].
90. P. Hut, *Phys. Lett.* **B69** (1977) 85; B. W. Lee and S. Weinberg, *Phys. Rev. Lett.* **39** (1977) 165; M. I. Vysotsky, A. D. Dolgov and Y. B. Zeldovich, *Pisma Zh. Eksp. Teor. Fiz.* **26** (1977) 200.
91. E. W. Kolb and K. A. Olive, *Phys. Rev.* **D33** (1986) 1202; E: **34** (1986) 2531; L. M. Krauss, *Phys. Lett.* **128B** (1983) 37.
92. R. Watkins, M. Srednicki and K. A. Olive, *Nucl. Phys.* **B310** (1988) 693.
93. K. Enqvist, K. Kainulainen and J. Maalampi, *Nucl. Phys.* **B317** (1989) 647.
94. K. Enqvist and K. Kainulainen, *Phys. Lett.* **B264** (1991) 367.
95. K. Griest and M. Kamionkowski, *Phys. Rev. Lett.* **64** (1990) 615.
96. P. Hut and K. A. Olive, *Phys. Lett.* **B87** (1979) 144.
97. D. Abbaneo *et al.* [ALEPH Collaboration], arXiv:hep-ex/0112021.
98. S. Ahlen, *et al.*, *Phys. Lett.* **B195** (1987) 603; D. D. Caldwell, *et al.*, *Phys. Rev. Lett.* **61** (1988) 510; M. Beck *et al.*, *Phys. Lett.* **B336** (1994) 141.
99. Ch. Weinheimer, et al, *Phys. Lett.* **B460** (1999) 219.
100. G. Steigman, K. A. Olive, and D. N. Schramm, *Phys. Rev. Lett.* **43** (1979) 239; K. A. Olive, D. N. Schramm, and G. Steigman, *Nucl. Phys.* **B180** (1981) 497.
101. K. A. Olive and M. S. Turner, *Phys. Rev.* **D25** (1982) 213.
102. S. H. Hansen, J. Lesgourgues, S. Pastor and J. Silk, *MNRAS* **333** (2002) 544 [arXiv:astro-ph/0106108].
103. R. D. Peccei and H. R. Quinn, *Phys. Rev. Lett.* **37** (1977) 1440; *Phys. Rev.*

D16 (1977) 1791; S. Weinberg, *Phys. Rev. Lett.* **40** (1978) 223; F. Wilczek, *Phys. Rev. Lett.* **40** (1978) 279.

104. J. E. Kim, *Phys. Rev. Lett.* **43** (1979) 103; M. A. Shifman, A. I. Vainshtein, and V. I. Zakharov, *Nucl. Phys.* **B166** (1980) 493; M. Dine, W. Fischler, and M. Srednicki, *Phys. Lett.* **104B** (1981) 199.
105. J. Preskill, M. B. Wise, and F. Wilczek, *Phys. Lett.* **120B** (1983) 127; L. F. Abbott and P. Sikivie, *Phys. Lett.* **120B** (1983) 133; M. Dine and W. Fischler, *Phys. Lett.* **120B** (1983) 137.
106. G. Raffelt, *Phys. Rep.* **198** (1990) 1.
107. D. Dearborn, D. N. Schramm, and G. Steigman, *Phys. Rev. Lett. 56* (1986) 26.
108. J. Ellis and K. A. Olive, *Phys. Lett.* **193B** (1987) 525; R. Mayle, J. Wilson, J. Ellis, K. A. Olive, D. N. Schramm, and G. Steigman, *Phys. Lett.* **203B** (1988) 188; **219B** (1989) 515; G. Raffelt and D. Seckel, *Phys. Rev. Lett.* **60** (1988) 1793; **67** (1991) 2605; A. Burrows, T. Ressel, and M. S. Turner, *Phys. Rev.* **D42** (1990) 1020; W. Keil, H. T. Janka, D. N. Schramm, G. Sigl, M. S. Turner and J. R. Ellis, *Phys. Rev.* **D56** (1997) 2419.
109. J. Wess and J. Bagger, *Supersymmetry and Supergravity*, (Princeton University Press, Princeton NJ, 1992); G.G. Ross, *Grand Unified Theories*, (Addison-Wesley, Redwood City CA, 1985); S. Martin, arXiv:hep-ph/9709356; J. Ellis, arXiv:hep-ph/9812235; K.A. Olive, arXiv:hep-ph/9911307 .
110. L. Maiani, *Proceedings of the 1979 Gif-sur-Yvette Summer School On Particle Physics*, 1; G. 't Hooft, in *Recent Developments in Gauge Theories, Proceedings of the Nato Advanced Study Institute, Cargese, 1979*, eds. G. 't Hooft *et al.*, (Plenum Press, NY, 1980); E. Witten, *Phys. Lett.* **B105**, 267 (1981).
111. J. Ellis, J.S. Hagelin, D.V. Nanopoulos, K.A. Olive and M. Srednicki, *Nucl. Phys.* **B238** (1984) 453; see also H. Goldberg, *Phys. Rev. Lett.* **50** (1983) 1419.
112. J. Rich, M. Spiro and J. Lloyd-Owen, *Phys.Rep.* **151** (1987) 239; P. F. Smith, *Contemp. Phys.* **29** (1998) 159; T. K. Hemmick *et al.*, *Phys. Rev.* **D41** (1990) 2074.
113. L. E. Ibanez, *Phys. Lett.* **137B** (1984) 160; J. Hagelin, G. L. Kane, and S. Raby, *Nucl., Phys.* **B241** (1984) 638; T. Falk, K. A. Olive, and M. Srednicki, *Phys. Lett.* **B339** (1994) 248 [arXiv:hep-ph/9409270].
114. see e.g. K.A. Olive and M. Srednicki, *Phys. Lett.* **205B** (1988) 553.
115. The LEP Collaborations, the LEP Electroweak Working Group, and the SLD Heavy Flavour and Electroweak Groups, CERN-EP-2000-016.
116. L. E. Ibáñez and G. G. Ross, *Phys. Lett.* **B110** (1982) 215; L.E. Ibáñez, *Phys. Lett.* **B118** (1982) 73; J. Ellis, D.V. Nanopoulos and K. Tamvakis, *Phys. Lett.* **B121** (1983) 123; J. Ellis, J. Hagelin, D.V. Nanopoulos and K. Tamvakis, *Phys. Lett.* **B125** (1983) 275; L. Alvarez-Gaumé, J. Polchinski, and M. Wise, *Nucl. Phys.* **B221** (1983) 495.
117. K.A. Olive and M. Srednicki, *Phys. Lett.* **B230**, 78 (1989); *Nucl. Phys.* **B355** (1991) 208.
118. ALEPH collaboration, D. Decamp *et al.*, *Phys. Rep.* **216** (1992) 253; L3 collaboration, M. Acciarri *et al.*, *Phys. Lett.* **B350** (1995) 109; OPAL collaboration, G. Alexander *et al.*, *Phys. Lett.* **B377** (1996) 273.

119. Joint LEP 2 Supersymmetry Working Group, *Combined LEP Chargino Results, up to 208 GeV*, `http://lepsusy.web.cern.ch/lepsusy/www/inos_moriond01/charginos_pub.html`.
120. K. Griest and D. Seckel, *Phys. Rev.* **D43** (1991) 3191.
121. J. Ellis, T. Falk, and K.A. Olive, *Phys. Lett.* **B444** (1998) 367 [arXiv:hep-ph/9810360]; J. Ellis, T. Falk, K.A. Olive, and M. Srednicki, *Astr. Part. Phys.* **13** (2000) 181 [Erratum-ibid. **15** (2001) 413] [arXiv:hep-ph/9905481].
122. M. E. Gómez, G. Lazarides and C. Pallis, *Phys. Rev.* **D61** (2000) 123512 [arXiv:hep-ph/9907261]; *Phys. Lett.* **B487** (2000) 313 [arXiv:hep-ph/0004028]; *Nucl. Phys.* **B638** (2002) 165 [arXiv:hep-ph/0203131]; R. Arnowitt, B. Dutta and Y. Santoso, *Nucl. Phys.* **B606** (2001) 59; T. Nihei, L. Roszkowski and R. Ruiz de Austri, *JHEP* **0207** (2002) 024 [arXiv:hep-ph/0206266].
123. C. Boehm, A. Djouadi and M. Drees, *Phys. Rev.* **D62** (2000) 035012; J. Ellis, K.A. Olive and Y. Santoso, *Astropart. Phys.* **18** (2003) 395 [arXiv:hep-ph/0112113].
124. M. Drees and M. M. Nojiri, *Phys. Rev.* **D47** (1993) 376; H. Baer and M. Brhlik, *Phys. Rev.* **D53** (1996) 59; and *Phys. Rev.* **D57** (1998) 567; H. Baer, M. Brhlik, M. A. Diaz, J. Ferrandis, P. Mercadante, P. Quintana and X. Tata, *Phys. Rev.* **D63** (2001) 015007; A. B. Lahanas, D. V. Nanopoulos and V. C. Spanos, *Mod. Phys. Lett.* **A16** (2001) 1229.
125. J. R. Ellis, T. Falk, G. Ganis, K. A. Olive and M. Srednicki, *Phys. Lett.* **B510** (2001) 236 [arXiv:hep-ph/0102098].
126. J. L. Feng, K. T. Matchev and T. Moroi, *Phys. Rev. Lett.* **84** (2000) 2322; J. L. Feng, K. T. Matchev and T. Moroi, *Phys. Rev.* **D61** (2000) 075005; J. L. Feng, K. T. Matchev and F. Wilczek, *Phys. Lett.* **B482** (2000) 388.
127. M. Battaglia *et al.*, *Eur. Phys. J.* **C22** (2001) 535 [arXiv:hep-ph/0106204]; see also: B. C. Allanach *et al.*, in *Proc. of the APS/DPF/DPB Summer Study on the Future of Particle Physics (Snowmass 2001)* ed. N. Graf, *Eur. Phys. J.* **C25** (2002) 113 [arXiv:hep-ph/0202233].
128. LEP Higgs Working Group for Higgs boson searches, OPAL Collaboration, ALEPH Collaboration, DELPHI Collaboration and L3 Collaboration, *Search for the Standard Model Higgs Boson at LEP*, ALEPH-2001-066, DELPHI-2001-113, CERN-L3-NOTE-2699, OPAL-PN-479, LHWG-NOTE-2001-03, CERN-EP/2001-055, arXiv:hep-ex/0107029; *Searches for the neutral Higgs bosons of the MSSM: Preliminary combined results using LEP data collected at energies up to 209 GeV*, LHWG-NOTE-2001-04, ALEPH-2001-057, DELPHI-2001-114, L3-NOTE-2700, OPAL-TN-699, arXiv:hep-ex/0107030; LHWG Note/2002-01, `http://lephiggs.web.cern.ch/LEPHIGGS/papers/July2002_SM/index.html`.
129. M.S. Alam *et al.*, [CLEO Collaboration], *Phys. Rev. Lett.* **74** (1995) 2885 as updated in S. Ahmed *et al.*, CLEO CONF 99-10; BELLE Collaboration, BELLE-CONF-0003, contribution to the 30th International conference on High-Energy Physics, Osaka, 2000; See also K. Abe *et al.*, [Belle Collaboration], [arXiv:hep-ex/0107065]; L. Lista [BaBar Collaboration], [arXiv:hep-ex/0110010]; K. Chetyrkin, M. Misiak and M. Munz, *Phys. Lett.* **B400**

(1997) 206 [Erratum-ibid. **B425** (1997) 414] [hep-ph/9612313]; T. Hurth, hep-ph/0106050; C. Degrassi, P. Gambino and G. F. Giudice, *JHEP* **0012** (2000) 009; M. Carena, D. Garcia, U. Nierste and C. E. Wagner, *Phys. Lett.* **B499** (2001) 141; P. Gambino and M. Misiak, *Nucl. Phys.* **B611** (2001) 338; D. A. Demir and K. A. Olive, *Phys. Rev.* **D65** (2002) 034007.

130. H. N. Brown *et al.* [Muon g-2 Collaboration], *Phys. Rev. Lett.* **86** (2001) 2227.
131. M. Knecht and A. Nyffeler, *Phys. Rev.* **D65** (2002) 073034; M. Knecht, A. Nyffeler, M. Perrottet and E. De Rafael, *Phys. Rev. Lett.* **88** (2002) 071802; M. Hayakawa and T. Kinoshita, arXiv:hep-ph/0112102; I. Blokland, A. Czarnecki and K. Melnikov, *Phys. Rev. Lett.* **88** (2002) 071803; J. Bijnens, E. Pallante and J. Prades, *Nucl. Phys.* **B626** (2002) 410.
132. G. W. Bennett *et al.* [Muon g-2 Collaboration], *Phys. Rev. Lett.* **89** (2002) 101804 [Erratum-ibid. **89** (2002) 129903] [arXiv:hep-ex/0208001].
133. M. Davier, S. Eidelman, A. Hocker and Z. Zhang, arXiv:hep-ph/0208177; see also K. Hagiwara, A. D. Martin, D. Nomura and T. Teubner, arXiv:hep-ph/0209187; F. Jegerlehner (unpublished, as reported in M. Krawczyk, *Acta Phys. Polon.* **B33** (2002) 2621 [arXiv:hep-ph/0208076].
134. J. R. Ellis, K. A. Olive and Y. Santoso, *New Jour. Phys.* **4** (2002) 32 [arXiv:hep-ph/0202110]..
135. Joint LEP 2 Supersymmetry Working Group, *Combined LEP Selectron/Smuon/Stau Results, 183-208 GeV*, `http://alephwww.cern.ch/~ganis/SUSYWG/SLEP/sleptons_2k01.html`.
136. A. B. Lahanas, D. V. Nanopoulos and V. C. Spanos, *Phys. Lett.* **B518** (2001) 94 [arXiv:hep-ph/0107151]; V. Barger and C. Kao, *Phys. Lett.* **B518** (2001) 117 [arXiv:hep-ph/0106189]; L. Roszkowski, R. Ruiz de Austri and T. Nihei, JHEP **0108** (2001) 024 [arXiv:hep-ph/0106334]; A. Djouadi, M. Drees and J. L. Kneur, JHEP **0108** (2001) 055 [arXiv:hep-ph/0107316]; H. Baer, C. Balazs and A. Belyaev, JHEP **0203** (2002) 042 [arXiv:hep-ph/0202076].
137. S. Heinemeyer, W. Hollik and G. Weiglein, *Comput. Phys. Commun.* **124** (2000) 76 [arXiv:hep-ph/9812320]; S. Heinemeyer, W. Hollik and G. Weiglein, *Eur. Phys. J.* **C9** (1999) 343 [arXiv:hep-ph/9812472]. M. Frank, S. Heinemeyer, W. Hollik and G. Weiglein, arXiv:hep-ph/0202166.
138. L. L. Everett, G. L. Kane, S. Rigolin and L. Wang, *Phys. Rev. Lett.* **86** (2001) 3484; J. L. Feng and K. T. Matchev, *Phys. Rev. Lett.* **86** (2001) 3480; E. A. Baltz and P. Gondolo, *Phys. Rev. Lett.* **86** (2001) 5004; U. Chattopadhyay and P. Nath, *Phys. Rev. Lett.* **86** (2001) 5854; S. Komine, T. Moroi and M. Yamaguchi, *Phys. Lett.* **B506** (2001) 93; J. Ellis, D. V. Nanopoulos and K. A. Olive, *Phys. Lett.* **B508** (2001) 65; R. Arnowitt, B. Dutta, B. Hu and Y. Santoso, *Phys. Lett.* **B505** (2001) 177; S. P. Martin and J. D. Wells, *Phys. Rev.* **D64** (2001) 035003; H. Baer, C. Balazs, J. Ferrandis and X. Tata, *Phys. Rev.* **D64** (2001) 035004.
139. M. Drees, M. M. Nojiri, D. P. Roy and Y. Yamada, *Phys. Rev.* **D56** (1997) 276 [Erratum-ibid. **D64** (1997) 039901] [arXiv:hep-ph/9701219]; M. Drees, Y. G. Kim, M. M. Nojiri, D. Toya, K. Hasuko and T. Kobayashi, *Phys.*

Rev. **D63** (2001) 035008 [arXiv:hep-ph/0007202]. V. Berezinsky, A. Bottino, J. R. Ellis, N. Fornengo, G. Mignola and S. Scopel, *Astropart. Phys.* **5** (1996) 1 [arXiv:hep-ph/9508249]; P. Nath and R. Arnowitt, *Phys. Rev.* **D56** (1997) 2820 [arXiv:hep-ph/9701301]; A. Bottino, F. Donato, N. Fornengo and S. Scopel, *Phys. Rev.* **D63** (2001) 125003 [arXiv:hep-ph/0010203]; V. Bertin, E. Nezri and J. Orloff, arXiv:hep-ph/0210034.

140. J. Ellis, K. Olive and Y. Santoso, *Phys. Lett.* **B539** (2002) 107 [arXiv:hep-ph/0204192].; J. R. Ellis, T. Falk, K. A. Olive and Y. Santoso, arXiv:hep-ph/0210205.
141. J. R. Ellis, A. Ferstl and K. A. Olive, *Phys. Lett.* **B532** (2002) 318 [arXiv:hep-ph/0111064].
142. J. R. Ellis, A. Ferstl and K. A. Olive, *Phys. Lett.* **481** (2000) 304 [arXiv:hep-ph/0001005].
143. J. R. Ellis, A. Ferstl and K. A. Olive, *Phys. Rev.* **D63** (2001) 065016 [arXiv:hep-ph/0007113].
144. J. R. Ellis and K. A. Olive, *Phys. Lett.* **B514** (2001) 114 [arXiv:hep-ph/0105004].
145. D. Abrams *et al.* [CDMS Collaboration], *Phys. Rev.* **D66** (2002) 122003 [arXiv:astro-ph/0203500].
146. A. Benoit *et al.*, *Phys. Lett.* **B545** (2002) 43 [arXiv:astro-ph/0206271].
147. DAMA Collaboration, R. Bernabei *et al.*, *Phys. Lett.* **B436** (1998) 379.
148. E. Accomando, R. Arnowitt, B. Dutta and Y. Santoso, *Nucl. Phys.* **B585** (2000)124 [arXiv:hep-ph/0001019]; A. Bottino, F. Donato, N. Fornengo and S. Scopel, *Phys. Rev.* **D63** (2001) 125003 [arXiv:hep-ph/0010203]; M. Drees, Y. G. Kim, T. Kobayashi and M. M. Nojiri, *Phys. Rev.* **D63** (2001) 115009 [arXiv:hep-ph/0011359]; Y. G. Kim and M. M. Nojiri, *Prog. Theor. Phys.* **106** (2001) 561 [arXiv:hep-ph/0104258]. A. B. Lahanas, D. V. Nanopoulos and V. C. Spanos, *Mod. Phys. Lett.* **A16** (2001) 1229 [arXiv:hep-ph/0009065]; A. B. Lahanas, D. V. Nanopoulos and V. C. Spanos, *Phys. Lett.* **B518** (2001) 94 [arXiv:hep-ph/0107151]. M. E. Gómez and J. D. Vergados, *Phys. Lett.* **512** (2001) 252 [arXiv:hep-ph/0012020].
149. J. Ellis, J. L. Feng, A. Ferstl, K. T. Matchev and K. A. Olive, *Eur. Phys. J.* **C24** (2002) 311 [arXiv:astro-ph/0110225].
150. CDMS Collaboration, R. W. Schnee *et al.*, *Phys. Rep.* **307** (1998) 283.
151. CRESST Collaboration, M. Bravin *et al.*, *Astropart. Phys.* **12** (1999) 107.
152. H. V. Klapdor-Kleingrothaus, arXiv:hep-ph/0104028.
153. G. Jungman, M. Kamionkowski and K. Griest, *Phys. Rep.* **267**(1996) 195; `http://t8web.lanl.gov/people/jungman/neut-package.html`.